Geochimica et Cosmochimica Acta 352 (2023) 175–193

Contents lists available at ScienceDirect

Geochimica et Cosmochimica Acta

journal homepage: www.elsevier.com/locate/gca

Titanium transport and isotopic fractionation in the Critical Zone

Sarah M. Aarons [a,b,*], Nicolas Dauphas [a], Nicolas D. Greber [c,d], Mathieu Roskosz [e], Julien Bouchez [f], Tamara Carley [g], Xiao-Ming Liu [h], Roberta L. Rudnick [i], Jérôme Gaillardet [f]

[a] Origins Laboratory, Department of the Geophysical Sciences and Enrico Fermi Institute, The University of Chicago, Chicago, IL 60637, USA
[b] Scripps Institution of Oceanography, University of California San Diego, CA 92093, USA
[c] Muséum d'histoire Naturelle de Genève, Route de Malagnou 1, CH-1208 Genève, Switzerland
[d] Institut für Geologie, Universität Bern, 3012 Bern, Switzerland
[e] IMPMC, CNRS, UMR 7590, Sorbonne Universités, Université Pierre et Marie Curie, Muséum National d'Histoire Naturelle, CP 52, 57 rue Cuvier, Paris F-75231, France
[f] Université de Paris, Institut de Physique du Globe de Paris, CNRS, Paris, France
[g] Department of Geology and Environmental Geosciences, Lafayette College, Easton, PA, USA
[h] Department of Geological Sciences, University of North Carolina-Chapel Hill, NC 27599-3315, USA
[i] University of California Santa Barbara, Department of Earth Science and Earth Research Institute, Santa Barbara, CA 93106, USA

ARTICLE INFO

Associate editor: Weiqiang Li

Keywords:
Titanium isotopes
Isotope fractionation
Chemical weathering
Particle transport
Chemical mobility

ABSTRACT

Stable Ti isotopes have been applied in the detrital sediment record to reconstruct the bulk composition of Earth's continental crust due to the relationship between magmatic differentiation and Ti isotopic compositions. However, no study has systematically evaluated the influence of provenance, physical, and chemical weathering on the composition of sediments relative to the protolith they originated from. To test the influence of these processes on Ti isotopic compositions we investigate the Ti isotope composition of 82 surface samples including loess, volcaniclastic rocks, river sediment, and two separate weathering profiles through igneous rocks, collected from a broad geographical area and a range of environmental conditions. Limited but significant Ti isotope fractionation exists in samples subjected to extreme chemical weathering processes, potentially as a result of elemental mobilization. For example, the δ^{49}Ti isotopic composition of bauxites developed on Columbia River basalt varies by up to 0.1‰, becoming isotopically heavier with increasing weathering intensity. However, negligible variation in δ^{49}Ti was found in a second profile of saprolites developed on weathered diabase. Titanium isotope variations in loess do not correlate with chemical weathering intensity or size sorting, but may instead be related to the provenance of the sediment. We find that the δ^{49}Ti of Amazon River sediments is correlated with the Al/Zr ratio, indicating that δ^{49}Ti is impacted by sediment sorting. At our study sites, the river averaged offset between the isotopic composition of the bedload and the suspended sediment fraction is 0.051‰, with the largest offset being + 0.116‰. Our data suggest that during chemical weathering, heavy Ti isotopes are preferentially incorporated into secondary minerals producing higher δ^{49}Ti in intensely weathered soils. During fluvial transport, the Ti isotopic composition of fine-grained sediment is heavier than that of its coarser counterpart. Crustal protolith composition and sorting during transport and sedimentation have a stronger effect on the Ti isotopic composition than chemical weathering. Our results have implications for studies that utilize the Ti elemental concentration to calculate relative enrichment or depletion during chemical weathering and physical transport processes in the Critical Zone and for studies using Ti isotopes in terrigenous sediments to infer the composition of their provenance.

1. Introduction

The composition of rocks exposed at Earth's surface, and their modification through chemical weathering and physical transport control the transport of sediment and nutrients from the continents to rivers and the oceans. The history of continental crust growth and its geochemical evolution are therefore tied with the carbon cycle and Earth's long-term habitability, by influencing biological productivity, organic carbon burial, and atmospheric CO_2 partial pressure (Berner et al., 1983). The extent and composition of the continental

* Corresponding author.
E-mail address: smaarons@ucsd.edu (S.M. Aarons).

https://doi.org/10.1016/j.gca.2023.05.008
Received 15 June 2022; Accepted 8 May 2023
Available online 16 May 2023

crust—whether it is predominately mafic or felsic—and the timing of plate tectonic initiation has broader implications for the delivery of critical nutrients from the continents to the oceans, impacts atmospheric composition, and is a control on Earth's long-term climate (Kasting & Catling, 2003; Lee et al., 2016; Alcott et al., 2022).

Reconstructing the composition of the continental crust through Earth's history is difficult because of possible preservation biases, the scarcity of ancient crustal remnants, and their modification by geological processes over billions of years. Detrital sedimentary rocks are often used to circumvent those difficulties as they may provide an average the composition of the upper continental crust over large drainage basins (Condie, 1993; Rudnick and Gao, 2003; Taylor and McLennan, 1985). Insoluble element concentrations and isotopic ratios of shales have been used to estimate the composition of the emerged continental crust exposed to physical and chemical weathering, and to determine whether early continental crust was predominantly mafic or felsic (Condie, 1993; Large et al., 2018; Smit and Mezger, 2017; Tang et al., 2016; Taylor and McLennan, 1985; Greber et al., 2017a; Ptáček et al., 2020).

Recently, non-traditional stable isotopes (e.g., Mo, Ti, Zr, V) have been analyzed in shales and glacial diamictites to reconstruct and understand the evolution of the average composition and oxidative weathering of Earth's upper continental crust (Greaney et al., 2020; Greber et al., 2017a; Tian et al., 2021; Tian et al., 2023). The isotopic composition of titanium (Ti) has been shown to vary systematically with magmatic differentiation (Millet et al., 2016; Deng et al., 2019; Johnson et al., 2019; Hoare et al., 2020), and because Ti is mostly insoluble during water–rock interactions (Orians et al., 1990), the Ti isotopic composition of detrital sediments can provide insights into the composition of their provenance (Greber et al. 2017a; Klaver et al., 2021). More recent studies have revealed more complicated Ti isotopic behavior during magmatic differentiation (Deng et al., 2019; Johnson et al., 2019; Hoare et al., 2020; Zhao et al., 2020) with variations associated with tectonic setting, and potentially water content and oxygen fugacity (Hoare et al., 2020; Aarons et al., 2020). Reconstructions based on Ti isotopes and other elemental ratios yield a realistic composition for the modern continental crust (Greber and Dauphas, 2019; Greber et al., 2017a).

Major issues for studies relying on the Ti isotopes in terrigenous sediments to reconstruct the composition of the continental crust through time is the potential for chemical and/or isotopic fractionation during chemical weathering and physical transport processes in the Critical Zone (Klaver et al., 2021; He et al., 2022), which is where the topmost layer of Earth's crust interacts with the atmosphere, hydrosphere, and biosphere. Such processes include isotopic fractionation during dissolution and incorporation of dissolved Ti into fine-grained secondary phases, or mineral size sorting during transport. Titanium has low solubility in most aqueous fluids, resulting in very low dissolved concentrations (Orians et al., 1990) and a short residence time in the oceans (100–200 yrs in sub-Arctic Pacific Ocean, 800–900 yrs in the central gyre of the North Pacific, (Orians et al., 1990) and 780 yrs based on the riverine inputs (Skrabal, 1995). This low solubility has led to the use of Ti to normalize other elements in studies probing elemental mobility during chemical weathering (Nesbitt, 1979). However, Ti may be mobilized in intensely weathered tropical regoliths (Cornu et al., 1999) and Ti isotopes have been shown to fractionate in saprolites (He et al., 2022). Moreover, some Ti may be incorporated into fine (clay and silt) fractions (Garcia et al., 1994; Taboada et al., 2006) and this Ti can be decoupled from coarser Fe,Ti-oxide grains during mobilization from soil profiles and transport, potentially introducing Ti isotopic fractionation. Indeed, it has been suggested that the Ti isotope composition of detrital sediments from the Eastern Mediterranean Sea differ from their provenance due to hydrodynamical/density sorting of Fe,Ti-oxides (Klaver et al., 2021).

It is therefore important to probe the effects of chemical weathering and particle size sorting of sediment on the δ^{49}Ti isotopic composition of terrigenous sediment (δ^{49}Ti is defined as the departure in permil of the ^{49}Ti/^{47}Ti ratio of a sample relative to the ratio of the OL-Ti standard). The aims of this study are to:

1. Understand the magnitude and mechanisms of Ti isotopic fractionation during chemical and physical transport in the Critical Zone;
2. Improve our understanding of the suitability of using Ti isotopes as a proxy for reconstructing the continental crust composition in the past;
3. Reconstruct the average Ti isotopic composition of the present-day upper continental crust to serve as a baseline for assessing the extent to which the Ti isotope composition of marine detrital sediments may be fractionated by Ti mobilization and transport.

To these ends, we have analyzed samples from a variety of Earth surface environments and climate regimes (cold-temperate oceanic to tropical), including loess, river sediment, and two weathering profiles developed on distinct bedrock compositions. We use the loess data as an alternative archive to reconstruct the average Ti isotopic composition of the present-day upper continental crust compared to marine detrital sediments. We find that Ti isotopes fractionate to varying degrees, attributable either to changes in provenance, physical size sorting, and/or Ti mobilization in the colloidal phase during intense chemical weathering. We then use bulk geochemical compositions of these samples to identify the processes responsible for Ti isotope fractionation and transmission electron microscopy of the most intensely weathered soil profile to characterize the carrier phases of Ti. Collectively, this work provides guidance for the use of Ti isotopes for reconstructing the continental crust composition in the past and improves our understanding of the processes affecting Ti isotopes in sediments, secondary weathering products, and waters.

2. Samples

2.1. Loess

Because loess derives from physical weathering of large geographical areas, its composition is often assumed to approximate that of the upper continental crust. Indeed, loess is a fine-grained (silt-sized) aeolian sediment typically comprised of pulverized regolith produced by the advance of ice sheets during glacial periods (Catt, 2001). In addition, as loess forms during dry, cold glacial periods, it is typically not subjected to significant chemical weathering (Gallet et al., 1998; Taylor et al., 1983). The loess studied here come from a broad geographical area (Fig. 1a) including the Adventdalen Valley, Spitsbergen, Norway; the Scilly Islands, United Kingdom; Nantois section in Brittany, Port-Racine section in Normandy and St. Brieuc, all from France; Kaiserstuhl section, Rhine Valley, Germany; Kesselt section, Belgium; Kansas, United States; Pampean loess from Argentina, Banks Peninsula, New Zealand; and Jixian section, China (Table 2). Information on sampling, bulk composition, and detailed geochemistry of these samples can be found in Huang et al. (2013) for samples from Europe and China, and in Li et al. (2010) for samples from the United States and New Zealand.

2.2. Amazon River sediments

Suspended sediments transported by rivers offer an opportunity to sample the products of chemical weathering and the influence of physical transport at Earth's surface. Their compositions provide insights into the nature of eroded lithologies, erosion rates, climate, and topography (Berner and Berner, 1987). These sediments can be stored over long timescales on continents, or directly transported to marine environments (Gaillardet et al., 1999; Viers et al., 2009; Martin & Meybeck, 1979). The largest river system on Earth, the Amazon River, transports approximately 1000 Mt of sediment per year to the Atlantic Ocean (Wittman et al., 2011). The Amazon River drains the Andes mountain range before transitioning into the tropical lowland region

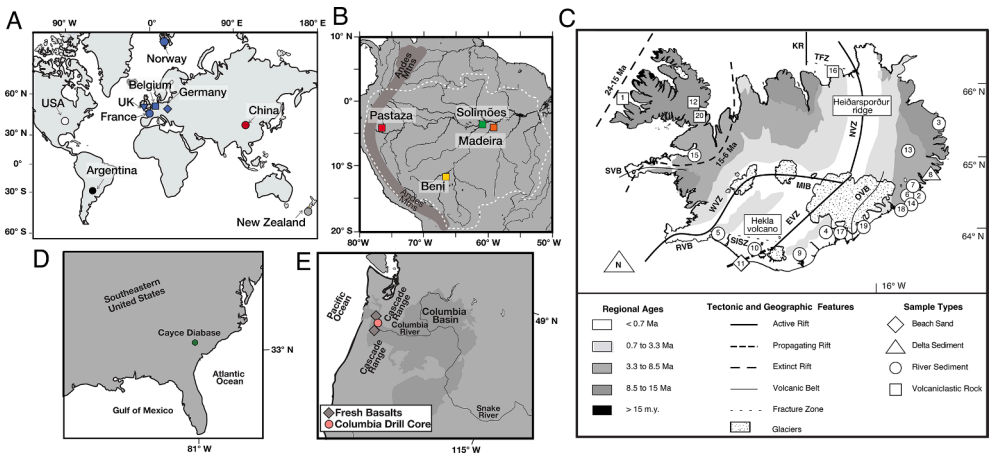

Fig. 1. Map showing the locations samples measured in this study. A) Locations of loess distributed across the world and the loess samples studied here (colored symbols) (adapted from (Huang et al., 2013; Pécsi, 1990)). B) Map showing the location of Amazon River basin and sediment sampling locations measured in this study. Colored symbols correspond to river tributary sampled and are used throughout remaining figures. Map adapted from Dellinger et al. (2014). C) Schematic map of Iceland modified from Carley et al. 2014. Ages of strata (modified from Thordarson and Hoskuldsson, 2002) and sample lithologies and locations are numbered (see Table 4). D) Geographic location of diabase dike in South Carolina. E) Map of Columbia River Basalt (gray area) and weathered sample sites studied here (pink circle and gray diamonds) (adapted from (Liu et al., 2013)). (For interpretation of the references to color in this figure legend, the reader is referred to the web version of this article.)

Table 1
Titanium isotope compositions of United States Geological Survey reference materials measured here.

Reference Material	Source	δ^{49}Ti (‰)	95% CI	n
BHVO-2	USGS	+0.015	0.028	44
BIR-1a	USGS	−0.052	0.029	28
G3	USGS	+0.441	0.027	44

underlain by the Guyana and Brazilian Precambrian shields in the east and a thick band of terrestrial sediments to the west (Fig. 1b). The two tributaries responsible for the largest sediment contributions to the Amazon River are the Solimões and the Madeira Rivers, both of which drain the Andes (Gibbs, 1967). The Madeira Basin primarily drains metasedimentary Paleozoic and Mesozoic rocks interspersed with outcrops of organic-rich shales and smaller areas of intrusive volcanic rocks (Carlotto et al., 1996). Metasedimentary to sedimentary rocks underlie the Andean section of the Solimões Basin, alongside exposed felsic to intermediate intraplate tholeiitic igneous rocks (Putzer, 1984; Rezende et al., 2021). The remaining tributaries in the lowland basin are sediment-poor and contain high dissolved organic matter concentrations.

Here we focus on sediments from four tributaries: the Madeira River and one of its major tributaries, the Beni River (draining only sedimentary rocks; Dellinger et al., 2014), as well as the Solimões River (draining a mixture of sedimentary rocks and andesite rocks; Carlotto et al., 1996), together with one of its relatively minor tributaries, the Pastaza River, which carries sediments having a much stronger influence from volcanic and plutonic calc-alkaline igneous rocks in its catchment (Kerr et al., 2002) than other Andean rivers. The samples were collected during previous field campaigns aimed at investigating how bedrock composition and weathering intensity influences grain size by sampling river depth profiles, with typically smaller grain sizes at shallower sampling depths in the channel and larger grain sizes closer to the river bed. Detailed procedures regarding sampling protocol are in Bouchez et al. (2011a) and Dellinger et al. (2014). Previous studies report the physical characteristics (Bouchez et al., 2011b), elemental and isotopic (Li, Sr, Nd) compositions (Bouchez et al., 2010; Bouchez et al., 2011c; Dellinger et al., 2014), and organic carbon export (Bouchez et al., 2014) of these suspended sediments. Here, we analyze suspended sediments from these tributaries at variable depths to gain insight into the role of physical size sorting on sediment Ti isotopic compositions, as hydrologic processes naturally sort suspended sediment in large rivers.

2.3. *Icelandic river sediments, volcaniclastic rocks, delta sediments, and beach sand*

Iceland provides an ideal study site to probe how the weathering byproducts of evolved tholeiitic crust is recorded in the detrital sedimentary rock record. Iceland is a portion of mid-ocean ridge exposed

Table 2
Titanium isotopic compositions of loess samples measured in this study. Major element data and chemical index of alteration (CIA) are from previous studies (Chauvel et al., 2014; Gallet et al., 1998; Huang et al., 2013; Jahn et al., 2001; Taylor et al., 1983). Concentrations of trace elements are in μg/g.

Sample	Location	SiO_2 (wt%)	TiO_2 (wt%)	Al_2O_3 (wt%)	CIA	δ^{49}Ti (‰)	95% C.I.	n	Zr	Nb	Sc	Sc
LO94	Adventdalen Valley, Spitsbergen, Norway	79	0.61	10.85	60	0.156	0.033	9	7.85	213	11.6	8.73
SCIL	Scilly Islands, United Kingdom	84	0.57	8.50	65	0.124	0.027	11	7.40	356	10.2	6.46
PR	Port Racine, Normandy, France	78	0.44	6.23	55	0.087	0.033	9	6.44	343	7.77	6.01
NS4	Nantois section, Brittany, France	72	0.93	10.59	60	0.078	0.027	9	6	305	12	–
HOT	France	76	0.70	8.34	59	0.118	0.027	9	7.45	387	10.2	7.71
K1	Kaiserstuhl section, Rhine Valley, Germany	60	0.32	7.78	65	0.162	0.033	9	5.4	250	8.9	5.7
K14	Kesselt section, Belgium	–	–	–	–	0.159	0.027	9	9.99	593	15.9	10.9
Cy-4a-C	Kansas, United States	80	0.71	10.7	58	0.123	0.027	10	10	570	21	4.9
52–54	Pampean Loess, Argentina	70	1.09	13.59	65	0.089	0.027	9	8	290	16	–
BP-3	New Zealand	73	0.69	15.2	61	0.167	0.027	10	9.77	340	27	8.5
BP-1	New Zealand	73	0.57	15.8	59	0.138	0.027	10	11.1	370	12.4	8
JX-1	Jixian section, China	71	0.79	14.55	64	0.156	0.027	9	19.6	190	13.2	–
JX-8	Jixian section, China	70	0.85	14.74	65	0.159	0.027	9	11.7	222	11.4	–

Table 3
Titanium isotopic compositions of Amazon River suspended particulate matter (SPM) and river bedload measured in this study. Sample information and geochemical data are from Bouchez et al. (2011a). Concentrations of trace elements are in μg/g.

Sample	River	Sample type	Depth (m)	TiO_2 (wt %)	δ^{49}Ti (‰)	95% CI	$\delta^{49}Ti_{sample\text{-}avg\ bedload}$ (‰)	n	Al (x10^4)	Zr
AM05-06	Solimões	SPM	14	0.8	0.135	0.028	0.01	9	8.41	242
AM06-02	Solimões	Bedload	–	0.5	0.136	0.034		7	3.68	268
AM06-03	Solimões	Bedload	–	0.3	0.116	0.031		9	3.14	229
AM06-05	Solimões	Bedload	–	0.9	0.114	0.027		15	4.70	765
AM06-10	Solimões	SPM	22	0.8	0.185	0.032	0.06	7	8.60	215
AM06-11	Solimões	SPM	15	0.8	0.202	0.028	0.08	9	8.87	204
AM06-13	Solimões	SPM	5	0.8	0.196	0.028	0.07	9	9.76	193
AM06-15	Solimões	SPM	25	0.7	0.159	0.030	0.04	16	7.95	208
Average Solimões SPM					0.175	0.030				
Average Solimões bedload					0.122	0.090				
AM05-15	Madeira	SPM	23	0.9	0.194	0.031	0.05	12	10.4	188
AM05-18	Madeira	SPM	8	0.8	0.205	0.032	0.06	8	11.0	153
AM05-19	Madeira	SPM	3	0.8	0.217	0.028	0.07	9	11.2	134
AM05-24	Madeira	Bedload	–	0.8	0.192	0.028		9	7.32	250
AM06-37	Madeira	SPM	10	0.9	0.195	0.027	0.05	15	8.56	250
AM06-39	Madeira	SPM	11	0.9	0.196	0.028	0.05	9	8.86	224
AM06-43	Madeira	SPM	0	0.9	0.212	0.028	0.07	9	10.0	207
AM06-44	Madeira	Bedload	–	1.4	0.101	0.027		12	2.51	2508
Average Madeira SPM					0.203	0.010				
Average Madeira bedload					0.147	0.410				
AM01-14	Beni	Bedload	–	–	0.134	0.028		9	6.77	–
AM07-05	Beni	Bedload	–	0.5	0.189	0.032		8	3.80	228
AM01-16	Beni	SPM	0	–	0.232	0.027	0.07	15	10.7	176
AM07-06	Beni	SPM	7	0.8	0.180	0.028	0.02	9	6.85	473
Average Beni SPM					0.206	0.240				
Average Beni bedload					0.162	0.250				
AM08-36	Pastaza	SPM	0	0.9	0.111	0.032	0.020	7	9.70	161
AM08-37	Pastaza	Bedload	–	0.8	0.091	0.033		8	7.98	131

subaerially due to magmatic productivity associated with a mantle plume (Morgan, 1971; Sigmarsson and Steinthórsson, 2007), and experiences subpolar oceanic to tundra climate. Icelandic rocks have a clear tholeiitic affinity and provide an opportunity to study felsic rocks produced in a thickened oceanic crust setting. Indeed, approximately 10% of the rocks at Iceland's surface are felsic, making it one of the largest exposures of felsic oceanic rock on Earth (Jonasson, 2007). For this reason, Icelandic crust is frequently cited as a possible modern analog for ancient continental crust (Marsh et al., 1991; Sigmarsson et al., 1991; Jónasson, 1994; Bindeman et al., 2012; Willbold et al., 2009; Reimink et al., 2014), though Archean TTG and felsic magmas generated at oceanic plateaux have significantly different geochemical compositions (Martin et al., 2008; Carley et al. 2014).

We measured the stable Ti isotopic composition of 20 samples collected from river sediments, volcaniclastic rock units, deltaic sediments, and beach sand located throughout Iceland (Fig. 1c, Table 4). More details on these Icelandic samples are provided by Carley et al. (2014; 2020), where the trace element and isotopic (O, Hf, U-Th-Pb) compositions of zircons are reported. Samples were collected with the aim of capturing the diversity of ages and local tectonic environments (e.g., on-rift, off-rift) in Iceland. These Icelandic sediments are relatively coarse compared to fine-grained shales—a distinction that must be

Table 4
Titanium isotopic compositions and geochemical characteristics of Icelandic river sediments, volcaniclastic rocks, delta sediments, and beach sands (this study). Samples are described in Carley et al. (2014, 2020), the map # corresponds to the physical location noted in Fig. 1c. Concentrations of trace elements are reported in μg/g.

Sample	Sample type	River	Map #	SiO_2 (wt%)	TiO_2 (wt%)	δ^{49}Ti (‰)	95% CI	n	Th	Zr	Nb	Sc
IXSd-1b	Volcaniclastic rock	Selárdalur	1	55	2.53	0.184	0.028	9	3.4	288	42	32
ISFK	River sediment	Fauská	2	62	1.86	0.178	0.028	9	4.0	369	38	26
ISKK	River sediment	Krossá-Kækjudalsá	3	65	1.38	0.274	0.028	9	6.2	407	52	21
ISHVt	River sediment	Hverfisfljót	4	53	2.20	0.066	0.029	9	1.5	177	17	39
ISOLF	River sediment	Ölfusá	5	51	1.74	0.214	0.027	9	2.1	439	26	47
ISR	River sediment	Reyðará	6	62	1.92	0.227	0.029	7	4.5	379	40	22
ISHo	River sediment	Hofsá	7	56	2.33	0.118	0.029	9	2.7	282	27	33
ISB	Delta sediment	Breiðdalsvík	8	55	2.37	0.147	0.027	9	2.5	246	27	35
ISHMyr	River sediment	Skálm	9	53	3.47	0.124	0.029	9	3.8	339	49	25
ISM	River sediment	Markarfljót	10	54	2.28	0.179	0.030	7	3.9	352	47	22
ISML	Beach sand	Markarfljót (mouth)	11	50	2.58	0.105	0.027	9	2.2	217	26	38
IXH-1a	Volcaniclastic rock	Húsavikurkleif	12	62	3.19	0.067	0.030	7	1.8	228	35	49
ISLF	River sediment	Lagarfljót	13	57	2.20	0.085	0.030	7	2.2	239	24	33
ISJL	River sediment	Jökulsá I Lóni	14	56	2.33	0.133	0.027	9	2.4	314	26	34
ISMi	River sediment	Miðá	15	54	2.33	0.102	0.027	9	1.9	173	26	38
IXT-1b	Volcaniclastic rock	Tjörnes	16	49	2.57	0.144	0.029	9	2.1	206	27	41
ISSG	River sediment	Gigjukvisl	17	51	2.22	0.071	0.028	9	1.0	154	14	43
ISFJAR	River sediment	Fjarðarsá	18	62	1.77	0.150	0.029	6	4.1	331	34	26
ISF	River sediment	Fjallsá	19	54	2.36	0.219	0.029	9	3.7	315	39	30
IXKM	Volcaniclastic rock	Mokollsdalur	20	53	2.76	0.067	0.030	7	1.8	197	22	37

considered during data interpretation.

2.4. South Carolina saprolite

Saprolites are clay-rich regoliths formed during tropical to subtropical chemical weathering (White, 2003), typically located in the lower portion of soil profiles overlying crystalline bedrock. Saprolites are representative of deep chemical weathering of bedrock and are well suited to study how chemical weathering impacts elements and isotopes. Because saprolites preserve the textures of the original rock they formed from, they are interpreted to be representative of isovolumetric chemical weathering and suitable for studying the geochemical and mineralogical changes that occur during the conversion of parent rocks into weathered material (Gardner et al., 1978).

We analyzed 17 samples spanning 30 m from a saprolite profile developed on Paleozoic igneous rocks weathered in a temperate climate in South Carolina, USA (Fig. 1d; Table 5). The saprolite samples were taken from a section exposed in a quarry wall over a 10 m depth range through a metadiabase dike intruded into granite near Cayce, South Carolina (33°58.09′ N, 81°03.07′ W) (Fig. 1d). The unaltered metadiabase was sampled at 30 m depth. The diabase dike shows more intense weathering close to the surface, which diminishes with depth.

The saprolites formed during the Tertiary in a subtropical climate regime, and although there are no constraints on mean annual precipitation (MAP) and temperature (MAT) during the Tertiary, the modern-day MAP and MAT is 1,200 mm/yr and 18 °C respectively (Gardner et al., 1981; Rudnick et al., 2004). A shift in the oxidation state is observed at a depth of 2 m, with smectite (potentially Fe-bearing) observed in the oxidizing environment above 2 m and kaolinite observed below (Gardner et al., 1981; Greaney et al., 2021). The samples analyzed here are well-characterized geochemically and mineralogically (Gardner et al., 1981), and stable isotopic compositions of Li (Rudnick et al., 2004), Mg (Teng et al., 2010), K (Teng et al., 2020), Fe and Cu (S.-A. Liu et al., 2014a) were previously reported. The Cu and Fe isotopic data from these samples were interpreted to reflect scavenging of light Fe and heavy Cu onto Fe-oxides formed by oxidation of siderite (S.-A. Liu et al., 2014a). Here we analyzed pristine, unaltered bedrock and saprolite at varying stages of chemical weathering intensities to probe the effects of chemical weathering on stable Ti isotopic composition in an environment with a basaltic igneous bedrock composition under temperate climate.

2.5. Columbia River bauxites

Extreme chemical weathering of rock forms an Al-rich amorphous rock called bauxite. The Ti isotopic composition of bauxites offers the opportunity to identify potential Ti isotope fractionation during extreme chemical weathering. A total of 10 samples from drill cores through bauxite formed on Columbia River Basalts (CRBs) located on the western, wet side of the Cascade Range in Washington, USA were analyzed here. The geochemical composition and environmental conditions under which the bauxite formed are detailed in X.-M. Liu et al. (2013; 2014b). Briefly, the CRBs erupted in the Miocene and covered a large portion of southern Washington, north and eastern Oregon and western Idaho (Fig. 1e) (Tolan et al., 1989). While the CRBs lie on both the western and eastern sides of the Cascade Mountain Range (the CRBs erupted prior to formation of Cascade Mountain Range), bauxites only formed on the western side due to orographic effects. Locations west of the Cascades currently receive measurable rainfall 150 days/year and annual average precipitation ranging from 150 to 200 cm/year (Kohn et al., 2002). The MAT and MAP at the study site is ~ 11 °C and ~ 1,100 mm (https://www.wrcc.dri.edu) (Liu et al., 2013). The "Columbia drill core" reached a vertical depth of 7.9 m but did not penetrate the fresh unaltered basalt, which is Sentinel Bluffs (Fassio, 1990). Several samples of unaltered parental basalt (Fig. 1e) from the same flow were collected to characterize the original geochemical composition of the bedrock. The bauxites are composed of gibbsite, halloysite, kaolinite, goethite, maghemite; quartz occurs in the more surficial samples (Fassio, 1990; Liu et al., 2013), and the profile can be divided into two zones: an Fe-rich upper zone with variable amounts of iron pisolites, and an Al-rich lower zone composed of nodular gibbsite (Fassio, 1990). The bauxite profile has been analyzed for stable Li, Mg, K, and radiogenic Nd isotope

Table 5
Titanium isotopic compositions of saprolite samples from South Carolina (CIA and major and trace element data from Rudnick et al., 2004) and bauxite from the Columbia River basalt (CIA and major and trace element data from Liu et al., 2013). Concentrations of trace elements are in μg g^{-1} and concentration of TiO_2 is in weight percent.

Sample	Type	Depth (m)	TiO_2 (wt%)	CIA	δ^{49}Ti (‰)	95% CI	n	Th	Zr	Nb	Sc
M1	Saprolite	0.1	0.66	88	0.064	0.027	9	–	–	–	–
M3	Saprolite	0.5	0.88	88	0.058	0.028	9	–	–	–	–
M4	Saprolite	1	0.52	92	0.048	0.028	9	–	–	–	–
M5	Saprolite	1.5	0.64	90	0.041	0.028	9	–	–	–	–
M6	Saprolite	2	0.58	87	0.067	0.028	9	–	–	–	–
M7	Saprolite	3	0.77	95	0.071	0.028	9	–	–	–	–
M8	Saprolite	4	0.78	95	0.088	0.028	9	–	–	–	–
M9	Saprolite	5	0.81	93	0.076	0.028	9	–	–	–	–
M10	Saprolite	6	0.76	91	0.053	0.028	9	–	–	–	–
M11	Saprolite	7	0.55	54	0.078	0.028	9	–	–	–	–
M12	Saprolite	8	0.56	55	0.102	0.028	9	–	–	–	–
M13	Saprolite	9	0.72	71	0.080	0.028	9	–	–	–	–
M14	Saprolite	10	0.85	90	0.068	0.028	9	–	–	–	–
L14-8	Saprolite	10	0.57	49	0.087	0.028	9	–	–	–	–
L14-9	Saprolite	10	0.58	46	0.083	0.027	9	–	–	–	–
M15	Saprolite	11	0.73	88	0.062	0.028	9	–	–	–	–
M20	Diabase	30	0.48	45	0.104	0.027	9	–	–	–	–
5/1–4	Columbia drill core	2.74	3.35	98.5	0.141	0.028	9	61	618	58	27
5/1–6	Columbia drill core	3.96	3.23	99.3	0.178	0.028	9	24	–	56	32
5/1–8	Columbia drill core	4.57	6.46	98.9	0.064	0.030	9	77	727	81	28
5/1–10	Columbia drill core	5.49	10.78	99.2	0.074	0.028	9	126	887	140	28
5/1–12	Columbia drill core	6.71	8.54	99.3	0.059	0.028	9	127	942	84	42
5/1–14	Columbia drill core	7.32	10.0	99.6	−0.136	0.030	9	77	399	54	59
5/1–15	Columbia drill core	7.92	7.02	99.9	−0.001	0.028	9	10	–	45	86
2380	Sentinel Bluffs basalt	–	1.75	39	0.011	0.030	9	7	154	12	38
2170	Sentinel Bluffs basalt	–	1.75	40	0.039	0.031	9	0	159	10	37
SB-1	Sentinel Bluffs basalt	–	1.82	39	0.013	0.030	9	1	148	8	31

compositions (Chen et al., 2020; Liu et al., 2013; X.M. Liu et al., 2014b), and shows generally lighter Li and K and heavier Mg isotopic compositions with increasing degree of weathering.

3. Methods

3.1. Titanium chemistry and isotopic analyses

A total of 13 powdered loess samples (previously described in Huang et al., 2013), 22 Amazon river sediments (previously described in Bouchez et al., 2014; Bouchez et al., 2011b; Dellinger et al., 2014), 20 Icelandic volcaniclastic rock and river sediments (previously described in Carley et al., 2014; 2020), 10 bauxite samples (previously described in Liu et al., 2013; X.-M. Liu et al., 2014b), 17 saprolite samples (previously described in Gardner et al., 1981; Rudnick et al., 2004; Teng et al., 2010), and various geological reference materials were analyzed between June 2018 and March 2019 in the Origins Laboratory of the Department of the Geophysical Sciences at the University of Chicago (Tables 1-5). All represent individual samples from specific locations; no composites or mixtures were analyzed.

Methods for Ti chemistry and isotopic analysis of powdered samples have been described in detail previously (Millet et al., 2016; Zhang et al., 2011), and we use the modified methods described in Greber et al. (2017b), which uses an alkali-flux fusion to ensure sample homogeneity and complete dissolution of Ti in acid prior to separation using ion-exchange chromatography. Powdered samples and lithium metaborate flux were mixed in a proportion of 1:6. After flux fusion at 1100 °C for ten minutes, samples were crushed in a stainless-steel mortar and pestle and a shard containing at least 20 μg of Ti was double spiked with a mixed ^{47}Ti-^{49}Ti solution following the ideal sample-spike proportions described in Millet and Dauphas (2014) and dissolved in HNO_3. The Ti double spike allows for precise measurement of Ti isotopic composition, corrects for any fractionation that may have occurred during purification, and accounts for instrumental mass bias. The dissolved double-spiked samples were then separated following procedures outlined by Zhang et al. (2011). The Ti isotopic composition of each sample was subsequently measured during four separate sessions on a Neptune multi-collector inductively coupled plasma mass spectrometer (MC-ICPMS) in the Origins Laboratory at the University of Chicago in medium resolution mode. Sample solutions, in a mixture of 0.3 M HNO_3 + 0.005 M HF, were introduced to the plasma using an Aridus I desolvating nebulizer. All sample analyses were bracketed with analyses of standards doped with the same double spike mixture used in the sample, with ^{48}Ti concentrations matched within ± 10% to that of the sample. Following a block of five samples, a blank solution was measured and used for on-peak baseline correction. Isotopic mass fractionation during purification and isotopic measurements of Ti were corrected using the double-spike technique (Millet and Dauphas, 2014). The reported Ti isotopic compositions of the samples are the average of standard-sample-standard bracketing, with the Ti isotopic composition of each bracket normalized by the mean isotopic composition of the bracketing standards (both samples and standards are corrected for mass fractionation using the double spike approach). The Ti isotopic composition of each sample is reported in δ^{49}Ti notation, which is the per mil deviation from the ^{49}Ti/^{47}Ti ratio of the Origins Laboratory Ti reference material (OL-Ti):

$$\delta 49Ti(‰) = \left(\frac{49Ti/47TiSample}{49Ti/47TiOL - Ti} - 1\right) \times 1000 \quad (1)$$

Uncertainty on the Ti isotopic measurements reported here (95% confidence interval (C.I.)) is assessed using methods described in Dauphas et al. (2009), which consider the instrument measurement session and the long-term external reproducibility. Specifically, the dispersion of the bracketing standards Ti isotopic compositions were used to estimate the instrumental uncertainty ($\sigma_{mass\ spec}$). Other uncertainty, such as the potential fractionation that could occur during sample dissolution and column chemistry separation ($\sigma_{unknown}$ = 0.013‰), is estimated through the long-term external reproducibility of geological reference materials. The total uncertainty of a measurement is defined as 95% C.I.$=2 \bullet \sqrt{\sigma^2_{unknown} + \sigma^2_{massspec}}$ (Greber et al., 2017b). Several geological reference materials (basalts BHVO-2, and BIR 1a, and granite G3), were processed and measured as samples during the course of this study. In each session, the δ^{49}Ti compositions of the reference materials were consistent with expectations from previous studies. The geological reference material's δ^{49}Ti compositions measured here are compiled in Table 1 and are in good agreement with values previously reported (Millet and Dauphas, 2014; Millet et al., 2016; Greber et al., 2017b).

3.2. Transmission Electron Microscopy

Three samples of fresh basalt (SB-1) and bauxites (5/1–4, and 5/1–14) were examined by scanning transmission electron microscopy (STEM) to determine whether Ti originally hosted in silicates could form insoluble Ti-nanophases that could be mobilized. All three samples were powdered and dispersed in an ethanol solution in an ultrasonic bath. Several drops from this dispersion were then deposited on a copper grid covered with a carbon membrane. The samples were then analyzed by STEM using a JEOL 2100F operating at 200 kV at the Institut de Minéralogie, de Physique des Matériaux et de Cosmochimie at Sorbonne Université.

3.3. Laser ablation measurements

A total of 20 samples from Iceland (river sediments, volcaniclastic rocks, delta sediments, and beach sand) were analyzed for major and trace element concentrations at the University of Bern with a LA-ICP-MS on pressed powder pellets following the methods described in Peters and Pettke (2016). The USGS glass standard GSD-1G was used for instrument calibration and the USGS geological reference material BIR-1a (Icelandic basalt) was run as a secondary standard to check accuracy of the analysis. All data have been evaluated assuming that the sum of major oxides equals 100%. Based on results for BIR-1a, precision on major elements is generally better than 5%, and most trace elements better than 10%, though some show relatively large uncertainties (e.g., low concentrated U is 50%). Each sample was measured five times to ensure reproducibility and we report the average of these five measurements as the result (Table S1).

4. Results

The Ti isotopic compositions of the samples analyzed in this study are presented in Tables 1-4.

4.1. Titanium isotopic composition of loess

The Ti isotopic compositions (hereafter referred to as δ^{49}Ti (‰)) of loess range from + 0.078 to + 0.167‰ (Fig. 2), defining an average of δ^{49}Ti = + 0.132 ± 0.029‰ (95% C.I.). In Table 2, we compile the TiO_2, SiO_2, Th, Zr, Nb, and Sc concentrations, as well as chemical index of alteration of the loess analyzed here. We find no clear correlation between these indices, which could reflect control of the Ti isotopic composition by magmatic differentiation or physical transport processes. The average loess Ti isotopic composition is similar to, albeit slightly lower than the average composition of terrigenous sediments (shales) with depositional ages from ~ 3.5 Ga to present (δ^{49}Ti =+0.183 ± 0.030‰ (95% C.I.), Greber et al., 2017a). A *t*-test comparing the two datasets (Ti isotopic composition of loess and < 3.5 Ga shales) indicates a p-value of 0.009, which suggests a slight statistically significant difference (<0.05) between the Ti isotopic composition of the upper continental crust from shales and loess.

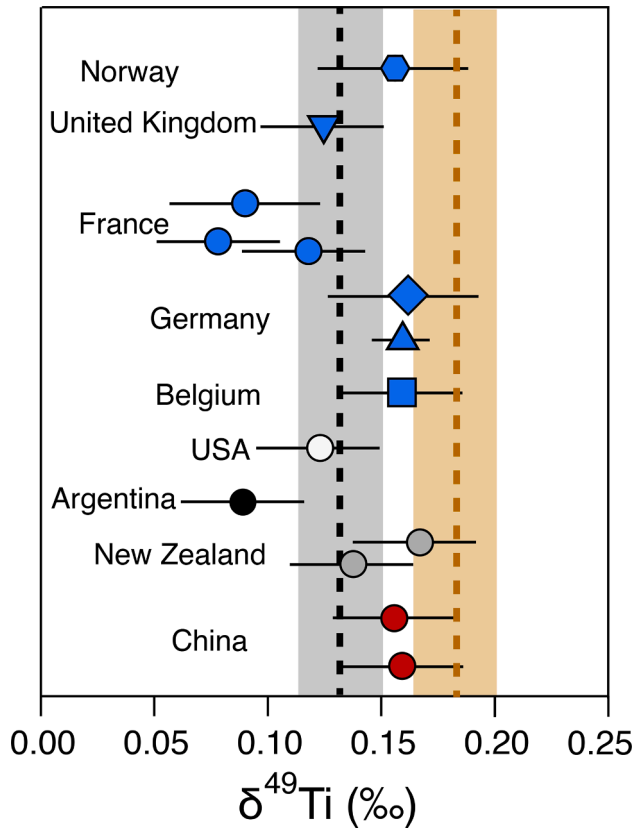

Fig. 2. Titanium isotopic composition of loess samples (colored symbols), average loess Ti isotopic composition (dashed black line with gray area indicating the ± 95% C.I.), and average < 3.5 Ga shale Ti isotope composition (dashed brown line with opaque brown area indicating the ± 95% C.I.; Greber et al., 2017a). Samples are color coded based on geographic origin: Europe (blue symbols), North American (white circle), South America (black circle), New Zealand (gray circles), and Asia (red circles). Similar shapes correspond to similar sample localities. Blue upright triangle is loess data from Germany (Mandl, 2019). The average Ti isotopic composition of loess shown in the figure does not include the data from Mandl (2019) which would slightly decrease the average from δ^{49}Ti = + 0.132 to + 0.129‰ respectively. (For interpretation of the references to color in this figure legend, the reader is referred to the web version of this article.)

4.2. Titanium isotopic compositions of river sediments

4.2.1. Amazon River sediments

Highly variable Ti isotopic compositions are observed in the suspended particulate matter (SPM) and bed sand samples collected from the Amazon River tributaries (Table 3). The δ^{49}Ti of SPM ranges from + 0.111 to + 0.232‰ whereas the bedload samples are generally lower in δ^{49}Ti, ranging from + 0.091 to + 0.192‰. The differences between the δ^{49}Ti values of SPM samples and the bedload for each sampling site are compiled in Table 3. SPM are on average + 0.054, +0.056, +0.044, and + 0.020‰ isotopically heavier than the corresponding bedload Ti isotopic compositions for the Solimões, Madeira, Beni, and Pastaza rivers, respectively. The Solimões River has an average SPM δ^{49}Ti composition of + 0.175‰ and bedload composition of + 0.122‰; the Madeira River SPM measures + 0.203‰ and bedload is + 0.147‰; the Beni River has an average SPM of + 0.206‰ and bedload composition of + 0.162‰; the samples from the Pastaza River have δ^{49}Ti compositions of + 0.111‰ (SPM) and + 0.091‰ (bedload). There is no discernible systematic trend in δ^{49}Ti values of suspended sediment with sampling depth in the river (Fig. 3, Table 3).

4.2.2. Titanium isotopic composition and bulk geochemistry of Icelandic sediments

The bulk composition of Icelandic volcaniclastic rocks and river sediments measured here do not mirror the magmatic array of Icelandic igneous rocks (Fig. 4). The sediments have δ^{49}Ti values from + 0.066 to + 0.274‰ (a range of 0.208‰) with an average δ^{49}Ti=+0.134 ± 0.06‰ (Table 4). The weighted average δ^{49}Ti of the river sediment and volcaniclastic rocks (based on the TiO_2 content of the sample) yields + 0.136‰. The samples do not show a discernible trend of δ^{49}Ti values with respect to MgO or SiO_2 content (Fig. 4a, b).

4.3. Titanium isotopic composition of weathering profiles

4.3.1. Gauging titanium mobility during weathering

The δ^{49}Ti values of two weathering profiles with different initial bedrock compositions from South Carolina and Washington (Table 5) were measured to compare variability in Ti fractionation with respect to initial Ti concentration, substrate, and environmental conditions. The South Carolina saprolites show uniform Ti isotopic composition (reduced χ^2 is 1.06, with a weighted average of 0.070 ± 0.016‰) (Fig. 5a). This composition is close to the metadiabase value of + 0.104 ± 0.027‰. Only one metadiabase measurement was performed, while 16 saprolite samples were analyzed, meaning that the δ^{49}Ti value of the latter is much better constrained. The Ti isotopic composition of the South Carolina saprolites show no discernible trend in isotopic fractionation with decreasing depth and are identical, within error, to the unweathered metadiabase (micro-gabbro) dike (Fig. 5a). No systematic trend in TiO_2 content with respect to weathering is observed, except that all weathered samples are more enriched in TiO_2 compared to the fresh bedrock (Table 5).

To evaluate elemental enrichment and depletion with respect to the unweathered parent rock, we use the mass transfer coefficient τ (Brimhall and Dietrich, 1987):

$$\tau_{Ti,j} = \frac{[Ti]_w/[j]_w}{[Ti]_p/[j]_p} - 1 \quad (2)$$

Where the subscripts *w* and *p* correspond to weathered and unweathered parent material, and *j* is the insoluble element used as a reference (in this case we use aluminum (Al), niobium (Nb) and zirconium (Zr) for comparison; Liu et al., 2013). When τ is positive, the element in the numerator (here Ti) has been added to the weathering profile, and when τ is negative it indicates elemental loss. There is a slight Ti enrichment in the saprolites towards the top of the profile (Fig. 5b).

By contrast, the bauxites developed on the Columbia River Basalt shows clear Ti elemental loss (relative to insoluble elements Nb and Zr) and isotopic fractionation compared to the fresh Sentinel Bluffs basalt (sample SB-1) throughout the weathering profile (Fig. 6, Table 5). Only at one depth (7.32 m, sample 5/1–14) a gain in Ti relative to Zr is observed (Fig. 6a). This sample also has the lightest Ti isotopic composition (δ^{49}Ti = -0.136‰; Fig. 6b). Given that considerable dissolved Zr (and to a much lesser degree Nb) concentration variability has been observed in the oceans (Firdaus et al., 2011), Nb may be a more suitable element for gauging elemental loss/gain. The δ^{49}Ti values range from −0.136 (sample 5/1–14, depth 7.32 m) to + 0.178‰ (sample 5/1–6, depth 3.96 m). The sample with the lightest Ti isotopic composition has the second highest TiO_2 concentration (Table 4) and the highest $\tau_{Ti,Nb}$ (excluding the fresh unaltered basalt) and $\tau_{Ti,Zr}$ values (including the fresh unaltered basalt; Fig. 6a).

4.3.2. TEM imaging insights into Ti carrier phases

Bauxites from the CRB weathering profile were analyzed and compared to a fragment of fresh Sentinal Bluffs basalt (SB-1) to determine the main Ti-carrier phases responsible for the observed Ti isotopic fractionation. The samples were evaluated on the individual powdered

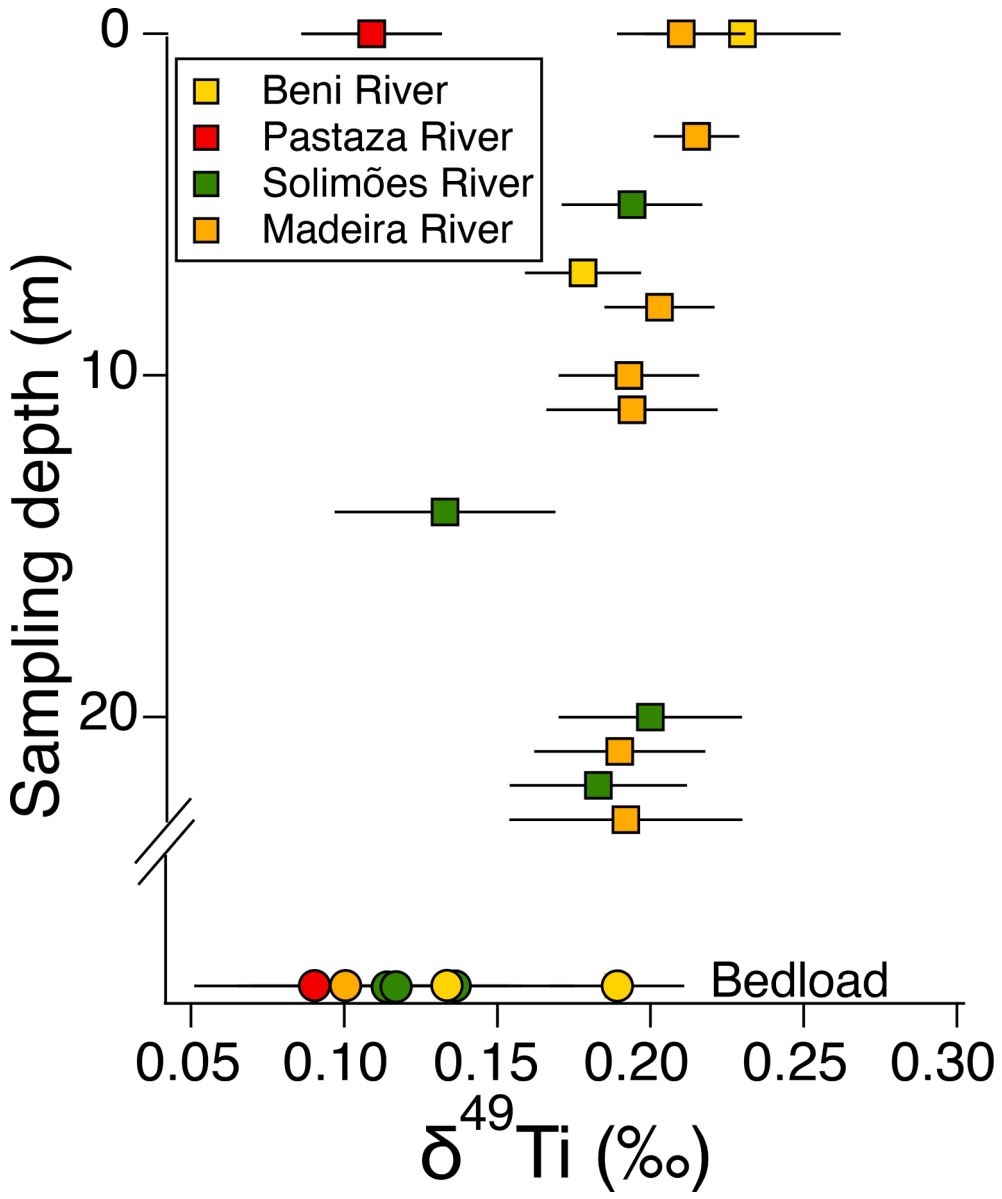

Fig. 3. Titanium isotopic compositions of suspended river sediments (colored squares) and river bedload (colored circles) from Amazon River tributaries with respect to sampling depth (m). River samples are distinguished by symbol color, see Fig. 2 for sampling locations within Amazon River basin. Symbols and color follow those outlined in Dellinger et al. (2014).

grain basis, with bauxite 5/1–14 being the coarsest-grained compared to the other two samples analyzed here (Fig. 7). Sentinel Bluff basalt (sample SB-1), assumed to be the unaltered parental rock, shows a homogenous distribution of elements throughout the fragment and a dense glassy texture (Fig. 7). Sample SB-1 contains only silicate minerals, with no colloidal, poorly crystallized minerals or clays. There are no significant Ti-bearing phases present in this sample, and Ti is found as a minor element present in the fragment imaged here. Notably, Ti is in very low abundance in this fragment. CRB lavas are characterized by generally fine grained clinopyroxene, plagioclase, and glassy residue, with hematite, apatite, ilmenite, and magnetite serving as accessory minerals, with textures ranging from intergranular to intersertal and occasionally hyalo-ophitic (Reidel, 1983). It is likely the Ti detected in this grain is a minor component in clinopyroxene. By contrast, bauxite 5/1–4 consists of much smaller particles with a loosely clumped texture compared to sample SB-1, with evidence of elemental mobility throughout the grain. Specifically, elements susceptible to release and loss during weathering such as Na, Cl, and K appear to concentrate in the outer portion of the grain, whereas Fe, O, and Ti are concentrated in the center of the grain and most likely represent an Fe,Ti-oxide (Fig. 7, see Fig. S3 for elemental spectra data). Bauxite 5/1–14 has a mottled distribution of elements associated with mobility (e.g., Na, Cl, K) and with hotspots concentrated in particular regions (Fig. 7). Some Ti-rich regions are present; however, these regions are not enriched in Fe or O. The Ti present in sample 5/1–14 is concentrated in a patchy, erratic pattern, which may hint at secondary Ti mineralization (Fig. 7). Based on the distribution of elements throughout the grain analyzed here, bauxite 5/1–4 appears to be more weathered compared to bauxite 5/1–14, consistent with it being the shallowest sample in the weathering profile.

5. Discussion

Understanding how chemical weathering, sedimentary transport processes, provenance and mixing may influence the Ti isotopic composition of fine-grained terrigenous sediments is essential for interpreting shale records in terms of the average crustal composition at

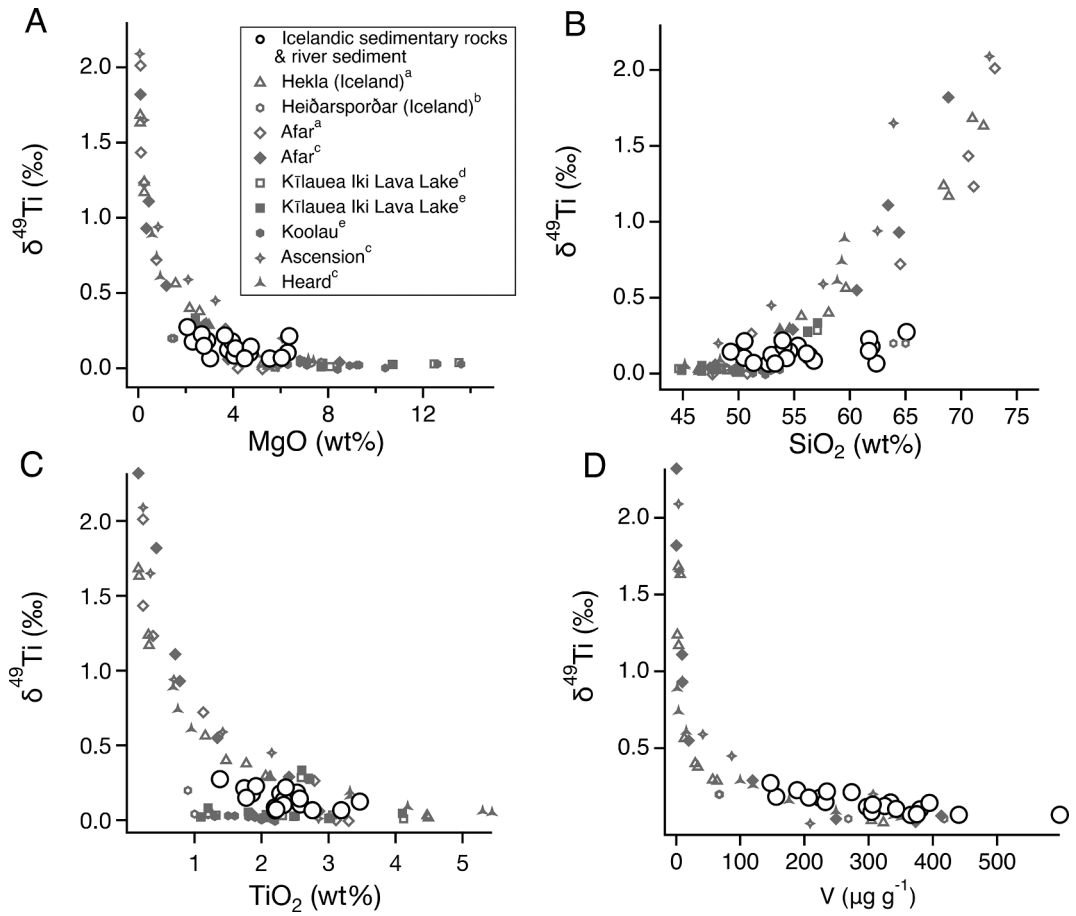

Fig. 4. Titanium isotopic compositions of Icelandic volcaniclastic rocks and river sediment (large white circles; this study) previously described in Carley et al. (2014) (A) with respect to MgO content, and previously measured intraplate differentiated igneous rocks (Ti isotopic data from [a]Deng et al., 2019; [b]Mandl, 2019; [c]Hoare et al., 2020; [d]Johnson et al., 2019; [e]Zhao et al., 2020; major and trace element data from Field et al., 2013; Chamberlain et al., 2019; Barling, 1990; Barling et al., 1994; Mancini et al., 2015; Deng et al., 2019; Johnson et al, 2019), (B) with respect to SiO_2 content, (C) with respect to TiO_2 content, and (D) with respect to vanadium concentration.

the time of deposition. We address each of these factors, in turn.

5.1. *Effect of provenance on titanium isotopic composition of terrigenous sediments*

5.1.1. *Is loess δ^{49}Ti variability driven by provenance or sorting?*

The small Ti isotopic variation in loess most likely reflects differences in the provenance. For example, the Pampean loess sample from Argentina contains a significant amount of volcanic glass and plagioclase (Zárate and Blasi, 1993), and has one of the lightest Ti isotopic compositions measured of all loess samples, consistent with input from relatively undifferentiated igneous rocks. The strontium (Sr) and neodymium (Nd) isotopic compositions of loess from China, Europe, and Argentina are reported in previous studies (Jahn et al., 2001; Taylor et al., 1983; Gallet et al., 1998). When compared to the measured Ti isotopic compositions, there is no discernible trend with Sr isotopic compositions, while the two samples with the lightest Ti isotopic compositions (52–54 and NS-4) have the most radiogenic Nd isotopic signatures (Fig. S1), consistent with the above suggestions. We further investigate the role of mineral sorting on Ti isotope compositions of terrigenous sediments via aeolian transport (loess), and fluvial processes (river sediments) in section 5.3.

5.1.2. *Influence of catchment rock types on Amazon River sediment*

Fractional crystallization removes Ti more efficiently from the melt compared to Zr and Al, giving rise to a negative correlation between Al/Ti and Ti/Zr ratios of igneous rocks (supplementary Fig. S2). However, data for the Amazon River sediment analyzed here show a positive correlation for these ratios, indicating that the variations do not reflect the sedimentary provenance (supplementary Fig. S2). In particular, the spread in Al/Zr ratio, which broadly reflects variations in the proportions of Al-rich clay minerals versus Zr-rich minerals such as zircons, indicates that mineral sorting plays an important role in determining the sediments' composition (see Section 5.3).

It is notable that the suspended sediment of the Pastaza River—which drains a significant fraction of igneous rocks—is offset from the remainder of the river sediments with respect to its Ti isotopic composition and Ti/Zr and Al/Ti ratios. Although the composition of the provenance of this sediment is not well characterized, its composition is close to the average composition of igneous rocks from the Andes (calculated from the GEOROC database; Lehnert et al., 2000, see Table S3 for averages, medians, standard deviations and standard errors), and its δ^{49}Ti value is similar to that of andesite (defined as SiO_2 = 57–62 wt%, δ^{49}Ti=~+0.17‰; Millet et al., 2016; Greber et al., 2017; 2021; Hoare et al., 2020) that formed in subduction zone settings similar to the Andes. By contrast, elemental ratios and δ^{49}Ti values of suspended sediments in rivers draining catchments dominated by terrigenous sedimentary rocks (Madeira and Beni Rivers) are closer to the average composition of Phanerozoic shales (Greber et al., 2017; Greber and Dauphas, 2019; Rudnick and Gao, 2003), suggesting that both mineral sorting and lithology may exert an influence on the Ti isotopic compositions of riverine sediments (Fig. 8a). Because the composition of the

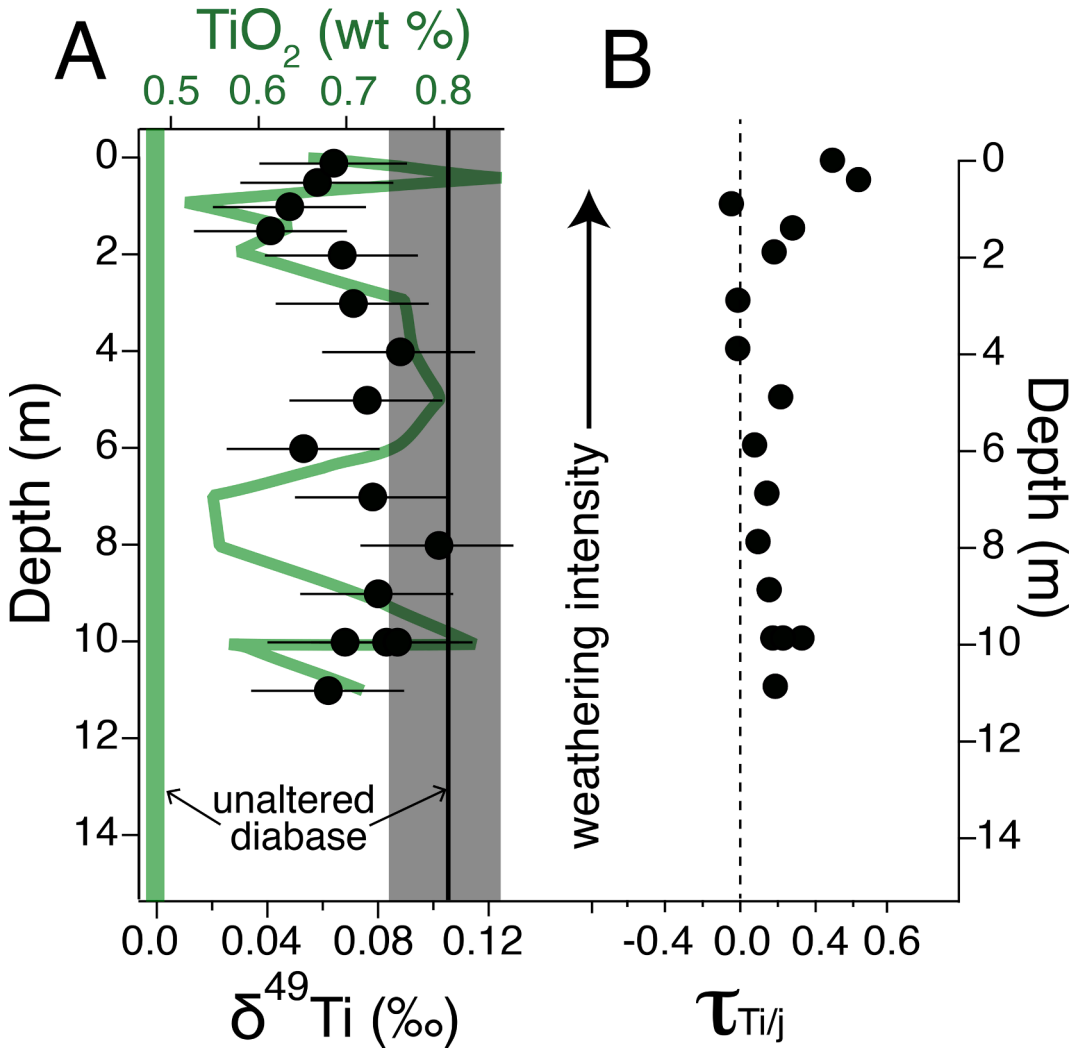

Fig. 5. (A) Titanium (this study) stable isotopic compositions (black circles) and TiO_2 (wt %; green trendline) of diabase samples from South Carolina. Unaltered diabase Ti isotopic composition represented by black line and the 95% C.I. is indicated by the lighter shaded gray area. The TiO_2 (wt %) of the samples are represented by green line, the unaltered diabase TiO_2 concentration is the thicker green line. (B) Enrichment/depletion index (τ) of Ti with respect to Al. Weathering intensity generally increases with decreasing depth. (For interpretation of the references to color in this figure legend, the reader is referred to the web version of this article.)

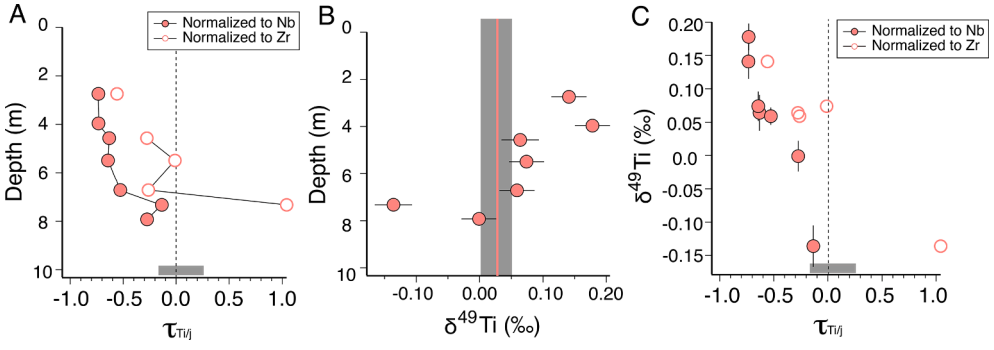

Fig. 6. Ti isotopic fractionation and depletion/enrichment in bauxite samples developed on Columbia River basalt. (A) Enrichment/depletion index (τ) of Ti with respect to immobile elements Nb and Zr, small gray bar indicates the range of several samples representing the unaltered parent material for both Nb and Zr (here we use the average of three basalts as representative of unaltered parent material). (B) δ^{49}Ti isotopic compositions of a bauxite from the Columbia River basalt with depth. Gray bar indicates range of δ^{49}Ti isotopic compositions of unaltered parent material, pink line is the weighted δ^{49}Ti isotopic composition of the weathering profile. (C) Correlation between δ^{49}Ti isotopic compositions and τ of Ti with respect to immobile elements Nb and Zr. Trace elemental concentration data from (Liu et al., 2013). Small gray bar indicates the range of several samples representing the unaltered parent material (samples SB-1, 2380, and 2170). (For interpretation of the references to color in this figure legend, the reader is referred to the web version of this article.)

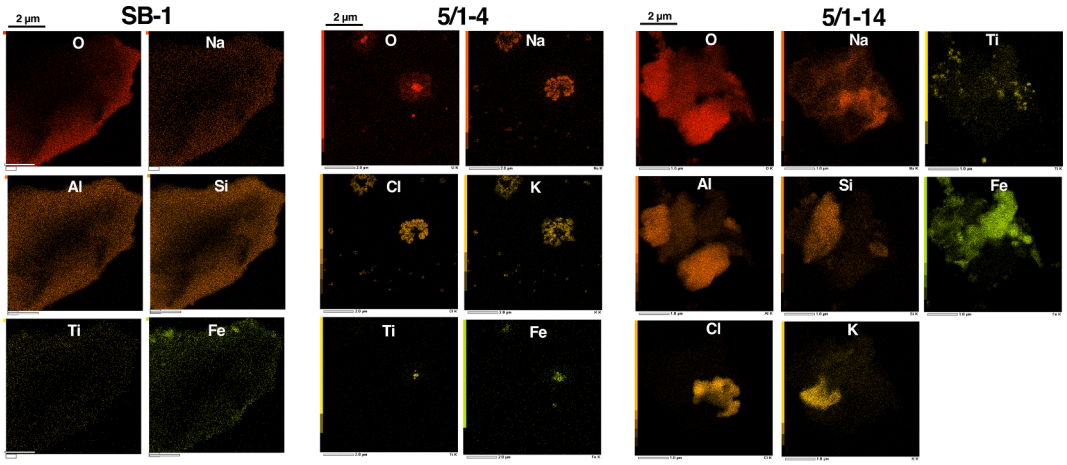

Fig. 7. Transmission electron microscopy (TEM) imaging results from two samples from the Columbia River bauxite (5/1–4 and 5/1–14) and unweathered Sentinal Bluff basalt (SB-1), which is the parental lithology upon which the bauxites developed. The EDX elemental maps are shown with the elemental spectrum in Fig. S3.

provenance is not well quantified for Amazon River sediments and is estimated using average compositions from the GEOROC database (Lehnert et al., 2000), it is unclear whether provenance or hydrodynamic sorting has the dominant control on Ti isotopic composition of these sediments.

5.1.3. Geochemical composition of weathered tholeiitic crust from Iceland

Igneous rock of tholeiitic affinity have higher δ^{49}Ti isotopic compositions at a given SiO_2 content (Deng et al., 2019), and terrigenous sediments derived from such rocks may also have higher δ^{49}Ti. To explore how weathering of tholeiitic source rocks influences detrital sediment geochemistry (Fig. 9) and the Ti isotopic composition of those sediments (Figs. 4 and 10, we have analyzed volcaniclastic rocks and river sediments from Iceland.

Although we lack parental host rock compositions to gauge the influence of chemical weathering on the observed Ti isotopic composition, the CIA is a useful indicator of mobile element loss. We find no discernible correlation between Ti isotopic composition and CIA (Fig. S4). In a plot of Ti isotopic composition of Icelandic volcaniclastic rocks and river sediments versus elements that track differentiation indices (Fig. 4), the Icelandic sediments follow the trends of intraplate differentiated igneous rocks with respect to MgO and V content (Fig. 4a, d), and, to a lesser degree, the TiO_2 content (Fig. 4c). This suggests that the Ti isotopic composition of Icelandic sediments reflect mixing of

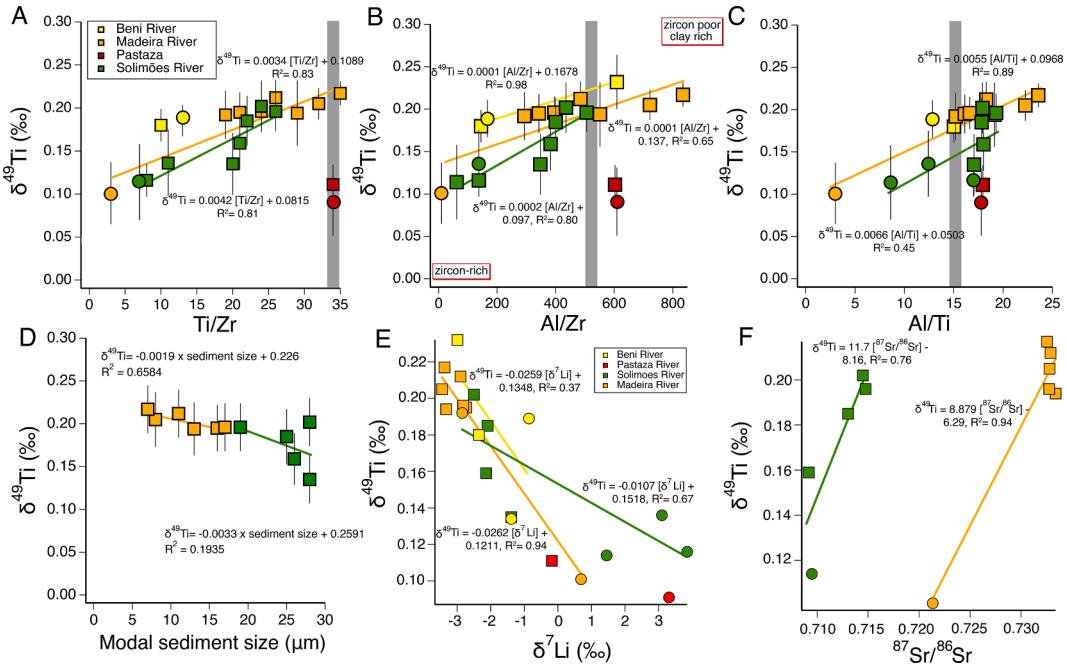

Fig. 8. Ti isotopic composition of suspended sediment (colored squares), bedload (colored circles) from the Amazon River relative to A) Ti/Zr, B) Al/Zr and C) Al/Ti ratios (μg g^{-1}/μg g^{-1}), which are proxies for fractionation between coarse/high density and fine/low density minerals. Linear regressions are separated by river source and show a good correlation with Ti/Zr ratio (R^2 = 0.83, 0.81), Al/Zr ratio (R^2 = 0.98, 0.65, 0.80) and to a lesser degree Al/Ti ratio (R^2 = 0.89, 0.45) with respect to the Ti isotopic composition. Gray bars are average compositions of Andean arc rocks from the GEOROC database (Lehnert et al., 2000). D) Ti isotopic composition of SPM relative to modal sediment size from Bouchez et al. (2011b). Linear regressions are separated by river source and show a weak correlation to modal sediment grain size (size that appears the most often in sample analyzed). E) Ti isotopic composition of SPM relative to Li isotopic composition and F) Ti isotopic composition of SPM relative to Sr isotopic composition. Elemental ratio data from Dellinger et al. (2014), Ti isotopic data from Table 2, Li isotopic data from Dellinger et al. (2014) and Sr isotopic data from Bouchez et al. (2010; 2011c).

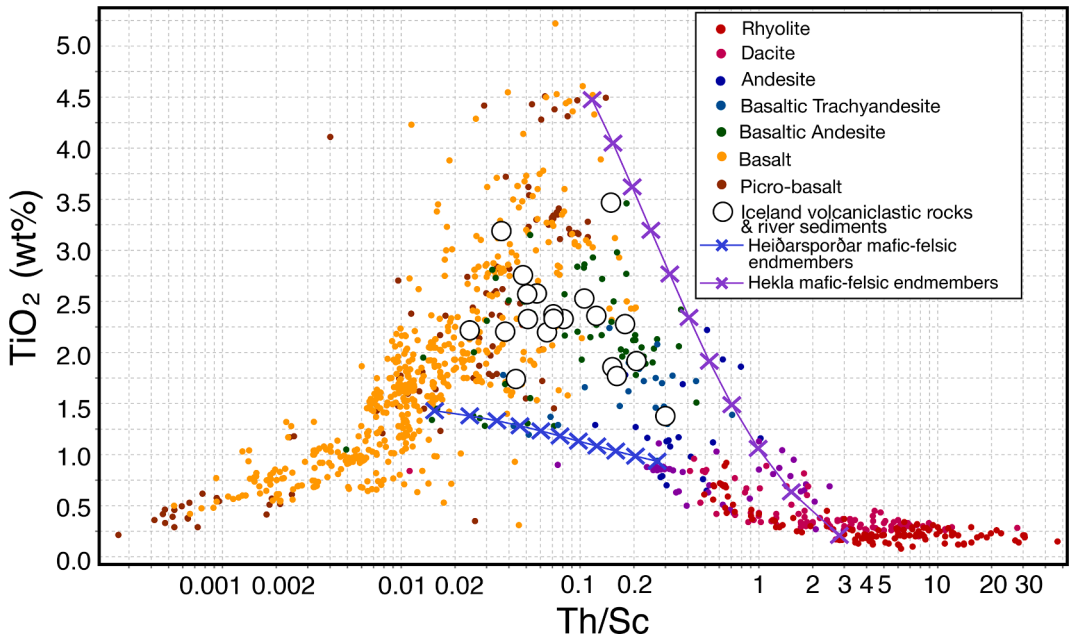

Fig. 9. Behavior of TiO_2 with respect to Th/Sc ratios in Iceland igneous rocks (color coded based on volcanic classification scheme ranging from picrobasalt to rhyolite, see Table S4), Icelandic sediment, and volcaniclastic rocks measured here (white circles), and mixing diagrams with different mafic and felsic endmember compositions based on Icelandic igneous rock compositions (lines with blue and purple x's; endmember compositions from Deng et al., 2019; Savage et al., 2011; Mandl, 2019; Mancini et al., 2015). (For interpretation of the references to color in this figure legend, the reader is referred to the web version of this article.)

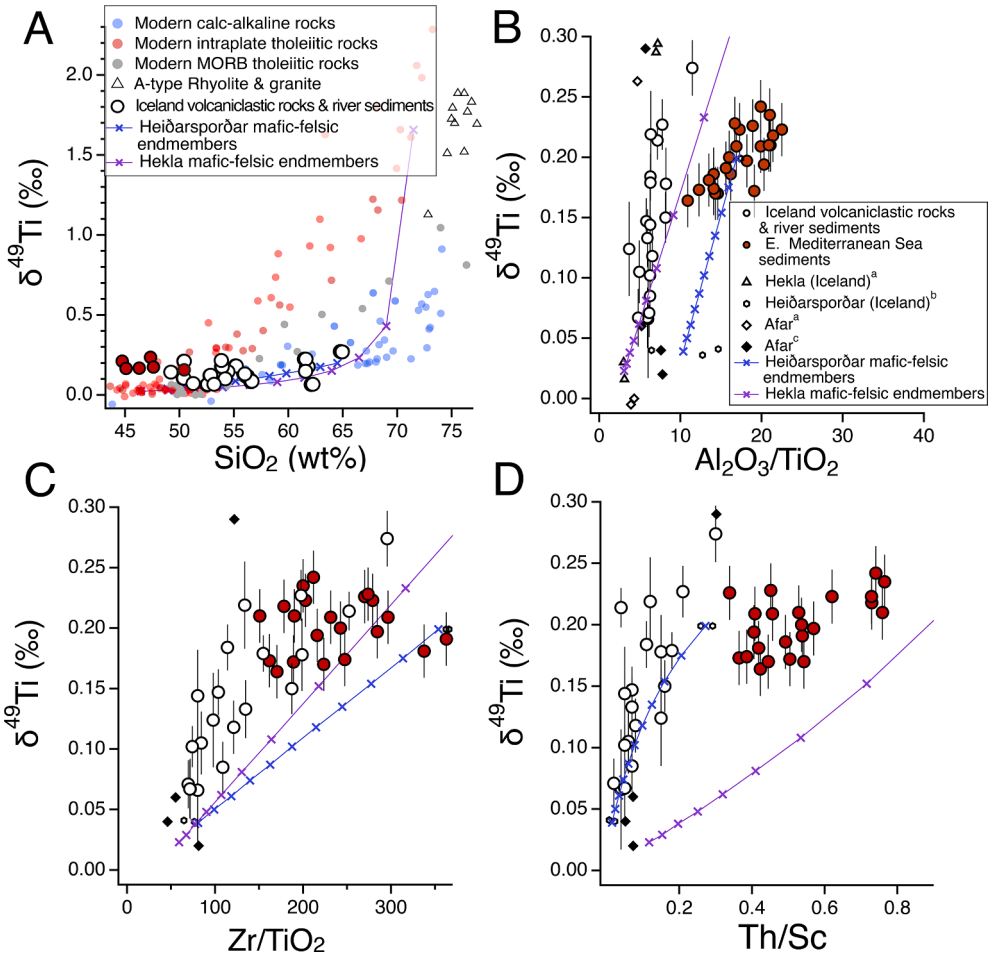

Fig. 10. Titanium isotopic compositions of Icelandic volcaniclastic rocks and river sediment along with calculated mixed proportions of mafic and felsic rocks from Iceland (endmember compositions from Deng et al., 2019; Savage et al., 2011; Mandl, 2019; Mancini et al., 2015), A) respect to SiO_2 content, and various igneous rock data from Aarons et al., 2020; Deng et al., 2018; 2019; Greber et al., 2017a,b; Hoare et al., 2020; Johnson et al., 2019; Millet et al., 2016; Zhao et al., 2020), B) with respect to the ratio of Al_2O_3/TiO_2 (proxy for grain size sorting) with Eastern Mediterranean sea sediments (Klaver et al., 2021; 2015) and intraplate igneous rocks (Ti isotopic data from [a]Deng et al., 2019; [b]Mandl, 2019, [c]Hoare et al., 2020), C) with respect to Zr/TiO_2 (proxy for grain size sorting) with intraplate igneous data, and D) with respect to Th/Sc with intraplate igneous rock data. Mixing calculations that represent varying proportions of mafic and felsic endmember material with low, high, and very high Ti concentrations are shown as yellow, green, and purple diamonds and lines. Intraplate igneous rocks include Hekla Volcano (white triangles), and Afar hotspot (open and closed diamonds). Symbols are the same in panels b, c, and d. (For interpretation of the references to color in this figure legend, the reader is referred to the web version of this article.)

mafic and felsic end members, or between igneous rocks at various stages of magmatic differentiation. When plotted against SiO_2 contents, the δ^{49}Ti of Icelandic sediments appear to lie on a trend defined by modern calc-alkaline igneous rocks, and are isotopically and geochemically in good agreement with end member mixing between mafic and felsic rocks from Heiðarsporður ridge, NE Iceland (Mandl, 2019; Mancini et al., 2015) and Hekla Volcano, Iceland (Deng et al., 2019; Savage et al., 2011).

To further explore the role of the provenance in setting the Ti isotopic composition of Icelandic sediments, we have calculated simple mixing scenarios between Icelandic felsic and mafic end members with varying Ti concentrations using data from previously published studies (Figs. 9 and 11; see Table S2 for end member compositions). The sediment geochemical compositions are plotted with available Icelandic igneous rock data (Deng et al., 2019; Mandl, 2019; Savage et al., 2011; Mancini et al., 2015; see Table S2), and with mixing ratios from 0 to 100% mafic-felsic end members in 10% increments. The mixing equation for major and trace element concentrations and Ti isotopic composition is as follows:

$$[C_i] = i \times [C_{felsic}] + (1 - i) \times [C_{mafic}] \quad (3)$$

Where $[C_i]$ is the concentration of a major or trace element at increment i, $[C_{felsic}]$ is the average concentration of the felsic endmember, and $[C_{mafic}]$ is the average concentration of the mafic endmember.

$$\frac{\delta^{49}T_{i_i} = i \times \delta^{49}T_{i_{felsic}} \times TiO_{2felsic} + (1 - i) \times \delta^{49}T_{i_{mafic}} \times TiO_{2mafic}}{i \times TiO_{2felsic} + (1 - i) \times TiO_{2mafic}} \quad (4)$$

Where $\delta^{49}Ti_i$ is the Ti isotopic composition at increment i, $\delta^{49}Ti_{felsic\ (mafic)}$ is the average Ti isotopic composition of the felsic (mafic) endmember, and $TiO_{2\ felsic\ (mafic)}$ is the average titanium oxide content of the felsic (mafic) endmember.

As is evident from the mixing calculations, several different mafic end members are needed to account for all the geochemical compositions of Icelandic sediments measured here (Fig. 9). We use this end member mixing scenario to explore variations in Ti isotopic compositions of Icelandic sediment as well (Fig. 10, see section 5.4).

5.2. Titanium isotopic fractionation during chemical weathering

5.2.1. Isotopic fractionation during extreme chemical weathering

Titanium is classically considered to be resistant to chemical weathering because of its low solubility in most aqueous systems. This makes it potentially well-suited for probing the geochemical evolution of Earth's continental crust through time. Titanium is frequently used as an immobile element to gauge elemental gains and losses within weathering profiles (Brewer, 1964; Brimhall and Dietrich, 1987). A recent study of saprolites developed on weathered tholeiitic basalt reported a small Ti isotopic fractionation during chemical weathering with δ^{49}Ti = -0.068 (0.057 2SD) to + 0.076 (n = 2, 0.050 and 0.052 2SD)‰ (He et al., 2022). Chemical extraction experiments indicated that the removal of crystalline Fe (hydr)-oxide phases can impart up to 0.2‰ lower δ^{49}Ti during chemical weathering (He et al., 2022). Other studies have documented the mobilization of Ti into solution before precipitation as anatase at low pH (<4.5) in the presence of organic acids (Cornu et al., 1999), and corrosion of Fe-Ti oxide minerals, such as ilmenite weathering to form pseudorutile, which then forms rutile (Grey and Reid, 1975) and/or anatase (Anand and Gilkes, 1984). Petrographic analyses of weathered soil profiles suggest the precipitation of anatase, which indicates Ti mobility at a small scale (millimeters; Cornu et al., 1999). Titanium isotopic fractionation is particularly likely in chemical weathering environments characterized by leaching, mineral dissolution, water transport, and during adsorption and mineral precipitation processes. We explore two such environments here—saprolites developed on a metadiabase from South Carolina, and bauxites developed on Columbia River basalts from the Pacific NW.

Titanium is commonly used to quantify element loss or gain during weathering because Ti is insoluble under most circumstances. However, because here we are interested in Ti mobility, such normalization is not an option and we instead use Nb for the bauxites:

$$f = [\mathrm{Ti/Nb}]_{\mathrm{bauxite}}/[\mathrm{Ti/Nb}]_{\mathrm{CRB}} \quad (5)$$

and Al for the saprolites:

$$f = [\mathrm{Ti/Al}]_{\mathrm{saprolite}}/[\mathrm{Ti/Al}]_{\mathrm{metadiabase}} \quad (6)$$

The saprolite profile shows no discernible trend in δ^{49}Ti with respect to chemical weathering intensity (Fig. S5) or depth, however there is an enrichment of Ti in the shallowest samples within the profile (Fig. 5). This enrichment is contrary to what is expected with increasing weathering intensity, and could be a result of aeolian input, though such input has yet to be documented in this profile. There is a redox discontinuity present at ~ 2 m depth, above which the environment becomes more oxidizing and Fe-rich smectite becomes the dominant clay species (Greaney et al., 2021). Thus, another possibility is that the increase in TiO_2 reflects its incorporation into smectite, though we lack the small-scale elemental (e.g., TEM imaging) context for evaluating this possibility. The Ti isotopic composition, however, is constant through

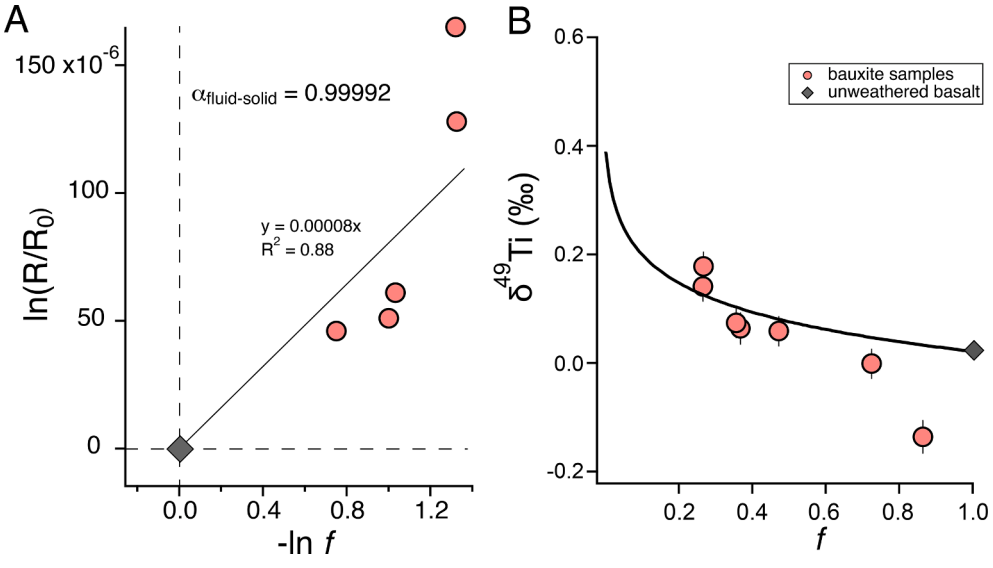

Fig. 11. δ^{49}Ti isotopic fractionation of weathered (pink circles) and average unaltered (gray diamond) Columbia River basalt bauxite samples. a) A Rayleigh distillation would follow a linear relationship when plotting ln (R/R_0) against -ln f, defining a slope equal to (1-α). Here, R and R_0 are the isotopic ratios ($^{49}Ti/^{47}Ti$) in weathered and unaltered Columbia River basalt respectively, f = $(Ti/Nb)_{sample}/(Ti/Nb)_{CRB}$ and is the amount of Ti remaining after removal during weathering and α is the Rayleigh fractionation factor associated with Ti incorporation into bauxite $(^{49}Ti/^{47}Ti)_{bauxite}/(^{49}Ti/^{47}Ti)_{fluid}$. We exclude two samples with negative δ^{49}Ti isotopic compositions from this panel. b) Ti isotopic compositions of bauxite samples against f. The black line depicts Ti removal via Rayleigh distillation for α = 1.0008. (For interpretation of the references to color in this figure legend, the reader is referred to the web version of this article.)

this interval and was not significantly affected by whatever process was responsible for the Ti enrichment.

By contrast, the bauxites show significant Ti isotopic fractionation associated with Ti elemental loss (Figs. 6 and 11). This isotopic fractionation can be modeled via Rayleigh distillation (Fig. 11). We normalize Ti concentration to Nb (see above) and model the δ^{49}Ti isotopic compositions of the weathered bauxites using the following equation:

$$\delta^{49}Ti_{bauxite} = (\delta^{49}Ti_{basalt} + 1000)\ f^{(\alpha-1)}\text{-}1000 \quad (7)$$

where f is defined in equation (5), and $^{\alpha}$ is the isotope fractionation factor associated with Ti incorporation into bauxite: $(^{49}Ti/^{47}Ti)_{bauxite}/(^{49}Ti/^{47}Ti)_{fluid}$, where we make the assumption that Ti is mobilized (at least locally) from primary minerals and precipitated into secondary minerals. These data can be modelled with a Ti isotopic fractionation of 0.05 to 0.10 ‰ (meaning that the solid is isotopically heavy relative to the fluid; Fig. 11b). However, one sample does not align with the general trend of increasing δ^{49}Ti compositions with respect to weathering (sample 5/1–14 δ^{49}Ti = -0.14‰). The possible reasons for the distinctively lighter δ^{49}Ti isotopic composition are discussed further below. The primary differences between the two weathering profiles are the initial petrology (basalt versus metadiabase) and the extent of weathering.

5.2.2. Origin of the Ti isotope fractionation in the bauxites

Titanium in unaltered Columbia River Basalt is likely hosted in glass, Fe,Ti-oxides, and clinopyroxene. Though they are resistant to alteration/leaching (Thompson et al., 2006), coarse Fe, Ti-oxides can be partially leached during weathering. By contrast, Ti in clinopyroxene and glass is readily mobilized when host silicate structures break down during aqueous alteration. This Ti can either be transported away as dissolved ions in the water, or precipitated locally in secondary insoluble phases. If those secondary solid phases are small, they can also be transported from the weathering profile as colloids.

The first explanation for the Ti isotope fractionation in the bauxite is that it is produced by selective dissolution of primary minerals that show inter-mineral isotopic fractionation. In igneous rocks, glass (and minerals crystallized late from silicate liquid) tend to have heavy Ti isotopic composition relative to Fe,Ti-oxides (Johnson et al., 2019; Hoare et al., 2020; 2022) due to the higher Ti-O coordination number of the latter (Aarons et al., 2021; Farges and Brown, 1997; Wang et al., 2020). Thus, one would expect the more readily-dissolvable Ti deriving silicates to have a heavy isotopic composition relative to less soluble Ti hosted in oxides, leaving behind an isotopically light regolith (e.g., He et al., 2022) – the opposite of what we observe (Fig. 6). However, if secondary minerals formed from this first pulse of silicate dissolution incorporated Ti, based on the experiments conducted by He et al. (2022) we would expect these minerals to have a heavier Ti isotopic composition, similar to what is observed, as the most weathered bauxites have the heaviest Ti isotopic composition. This is in agreement with the findings of He et al. (2022) who showed that crystalline Fe(hydro)-oxide mineral phases formed within weathered basalts are isotopically heavier than the substrate they originated from (He et al., 2022).

The speciation of Ti in Critical Zone waters is uncertain, but based on studies of dissolved Ti in seawater, we expect it to be $TiO(OH)_2$ (Orians et al., 1990). During conversion of rock into soil, some of the Ti released from partial mineral dissolution will be exported from the soil profile, while some will be adsorbed on mineral surfaces or will form secondary alteration phases. Titanium could be isotopically fractionated during this process. To better understand the possible controls on Ti isotopic fractionation during bauxite formation, we analyzed three of the Columbia River basalt samples via transmission electron microscopy (TEM): the unaltered basalt SB-1, bauxite 5/1–4 with the highest δ^{49}Ti (+0.141‰) and bauxite 5/1–14 with the lowest δ^{49}Ti (-0.136‰) (Table 5). We chose TEM because secondary Ti phases may be too small to be resolved with a scanning electron microscope (Ott et al., 2021). For each sample, we acquired several elemental STEM maps to identify areas rich in Ti, and electron diffraction patterns were collected to identify the mineralogical carriers of Ti (Fig. 7).

Previous studies using SEM have described high Ti-content phases (potentially identified as ilmenite) in the colloidal fraction of a series of weathered soils (Bern et al., 2011). Moreover, in Miocene fluvial deposits the weathering of detrital Fe-Ti oxides formed colloidal leucoxene, which is associated with organic matter (Weibel, 2003). In this study, all of the bauxites contain sodium and potassium chlorides, with colloidal to pseudocrystalline textures suggesting Ti mobility. In bauxites 5/1–4 and 5/1–14, an almost pure colloidal to microcrystalline likely TiO_2 oxide (with minor Fe) was observed via TEM/STEM (Fig. 7). Other Ti-rich grains in bauxite 5/1–14 are likely ilmenite (with a Ti/Fe ratio of close to 4/1). The difference in the single-grain distribution of Ti from the unaltered parent basalt (SB-1) to the more weathered bauxites (5/1–4 and 5/1–14) suggests mobility and redistribution of Ti during secondary weathering. Based on extraction experiments performed on saprolite samples (He et al., 2022), we expect secondary minerals such as Fe(hydro)-oxides to be enriched in the heavy isotopes of Ti, which we observe with increasing weathering intensity in our profile.

5.2.3. Alternative explanations for observed Ti isotopic fractionation in CRB bauxites

Past study of the CRB documented addition of eolian dust, based on lower $^{143}Nd/^{144}Nd$ ratios, higher Nd concentrations, the presence of quartz (which does not occur in unweathered CRB) and an increase in Li concentrations in the upper 5 m of the profile (Liu et al., 2013). The proportions of dust decreased with depth. The shift towards heavier Ti isotopic compositions compared to the unaltered basalt begins at 6.71 m depth to the shallowest sample at 2.74 m. Although we lack a representative sample of dust that is deposited in this location (likely Palous Hills), we would expect it to have a similar Ti isotopic composition to loess from North America (δ^{49}Ti=+0.123‰, Kansas, USA). The two uppermost samples observed in this profile have δ^{49}Ti between + 0.141 to + 0.178‰ at 2.74 m and 3.96 m depth, respectively. The average TiO_2 content of loess is 0.69 wt% (this study) whereas the average TiO_2 content of the bauxites is 7.06 wt%. Following the calculations of Liu et al. (2013), addition of approximately 40 wt% of dust to the top of the Columbia profile is required to explain the heavy Ti near the top of the profile, indicating that the addition of eolian material is unlikely to have had a strong influence on the δ^{49}Ti isotopic composition of the bauxites.

Another possible explanation for the large range in Ti isotopic compositions of the bauxites is that they developed on multiple lava flows that had distinctive δ^{49}Ti, rather than a single pulse of lava with homogeneous δ^{49}Ti. However, if this were the case, we might expect to see an abrupt change in δ^{49}Ti across the flow boundary. Instead, δ^{49}Ti increases steadily from bottom to top. Moreover, the CRB profile analyzed here formed on the Sentinel Bluffs Member of the Grande Ronde Basalt in Columbia County, Washington (Liu et al., 2013), which has been extensively characterized through borehole and stratigraphic mapping (Reidel et al., 1989). Borehole analyses of CRB's extending thousands of meters in depth demonstrate that the Sentinel Bluffs Member typically contains three to five flows with individual flow thicknesses ranging from tens to hundreds of m (Reidel et al., 1989). Because the bauxites analyzed here span a relatively small range in depth of ~ 5.2 m, we assume that all samples formed on a single flow.

5.3. Isotopic variability due to transport and mineral sorting

5.3.1. Influence of aeolian transport on Ti isotopic composition

Formation of loess requires aeolian transport and deposition, which may result in preferential size sorting due to density-driven fallout during atmospheric transport. Minerals present in sediment are of varying density, and the density-driven loss or accumulation of zircon or the enrichment of zircon due to their resistance to breakdown during

transport (known as the "zircon effect") has been documented to fractionate the hafnium isotopic compositions of bulk dust samples (Aarons et al., 2013) and periglacial loess (Taylor et al., 1983; Chauvel et al., 2014). Due to the relatively homogeneous Ti isotopic composition of samples analyzed here and its similarity to the average < 3.5 Ga shale δ^{49}Ti isotopic composition (Fig. 2), it is unlikely that accumulation of dense minerals during periglacial loess formation is driving the observed isotopic fractionation. The slight difference in Ti isotopic compositions between loess and shales could be potentially related to mineralogical sorting as a result of the depositional environment (terrigenous versus shallow marine), transport process (aeolian versus fluvial), or smaller sampling size of loess (n = 13) versus shales (n = 48). A combination of the < 3.5 Ga shale and loess data results in a δ^{49}Ti=+0.158‰, which may be a more accurate estimation of the UCC Ti isotopic composition.

5.3.2. *Influence of density and size sorting during fluvial transport on Ti isotopic composition*

5.3.2.1. Sediments from large rivers. Large rivers with geographically wide drainage areas incorporate weathering and erosion products that are broadly representative of the global continental surface. The Amazon River basin and the sediments from individual rivers measured here drain basins with mixed lithologies, ranging from Paleozoic to Tertiary sedimentary rocks in the Madeira and Beni (tributary of the Madeira) rivers to arc-derived andesite in the Solimões and Pastaza (tributary of the Solimões) rivers (Dellinger et al., 2014). The Ti contents and isotopic compositions of the Amazon River suspended sediment show subtle variations depending on locality and depth (Fig. 3). The small Ti isotopic fractionation reported here may reflect differences in bedrock lithology drained by the river systems, physical size sorting during fluvial transport, or the effect of chemical weathering. We use various geochemical proxies to disentangle these processes and evaluate how the Ti isotopic composition of the continents is fractionated by weathering and fluvial transport.

Shales are products of fluvial transport of terrigenous sediment that is ultimately deposited in a shallow marine environment. Their δ^{49}Ti values and chemical compositions have been used to reconstruct the composition of their source rocks. It is therefore imperative to understand how transport-induced size sorting or density-driven mineralogical changes impact geochemistry and isotopic compositions of these sedimentary archives. A previous study, focused on detrital sediments from the Eastern Mediterranean Sea, suggested that mineralogical changes associated with size and hydrodynamic sorting during riverine transport can bias the Ti isotopic compositions of fluvial sediments (Klaver et al., 2021). This study found that the removal of Fe,Ti- oxides due to density sorting may increase the δ^{49}Ti values of suspended sediment. This fractionation of Ti isotopes arises from the fact that Fe,Ti-oxides such as geikielite, pseudobrookite, rutile, ilmenite, and Ti-bearing silicate minerals such as titanite host Ti in six-fold coordination. Higher coordination (e.g., six-fold coordination) is associated with weaker bonds, favoring incorporation of lighter Ti isotopes into the mineral structure of dense Ti oxides relative to other phases (Aarons et al., 2021; Greber et al., 2021; Deng et al., 2019; Hoare et al., 2020; 2022; Johnson et al., 2019; Millet et al., 2016; Rzehak et al., 2021; 2022; Wang et al., 2020, Zhao et al., 2020). Here we explore the impact of density and size sorting during fluvial transport by comparing the δ^{49}Ti composition of river sediments to geochemical proxies of source material and size sorting: Al/Ti, Ti/Zr and Al/Zr ratios (in μg g^{-1}) (Greber and Dauphas, 2019; Klaver et al., 2021; Fig. 8 and supplementary Fig. S2).

The ratio of Al/Ti in sediments should indicate the proportion of clay-to Fe,Ti-oxide minerals. A positive correlation exists between δ^{49}Ti and Al/Zr (Fig. 8b) and Al/Ti (Fig. 8c), which we interpret as mixing between clays (with higher δ^{49}Ti) and higher density minerals (with lower δ^{49}Ti). Parallel trends are observed for each river, consistent with different drainage basin lithologies with specific δ^{49}Ti values. However, each river is similarly affected by density sorting. There is no statistically significant correlation between δ^{49}Ti values and the modal suspended particle size for the Solimões and Madeira Rivers (Bouchez et al., 2011b) (Fig. 8d), suggesting that the main Ti isotopic fractionation occurs between suspended and bedload sediments. Indeed, in individual rivers (Beni, Madeira, and Solimões Rivers), sediments enriched in coarser particles (the bedloads) are characterized by lower δ^{49}Ti values, and suspended sediments are characterized by higher δ^{49}Ti values. The isotopic difference between the δ^{49}Ti of the most clay-rich and zircon-rich (both defined by the Al/Zr ratio) sediments yield $\triangle^{49}$Ti = +0.115 (Madeira River), +0.082 (Solimões River), and + 0.043‰ (Beni River). Therefore, hydrodynamic sorting may impart a $\triangle^{49}$Ti of nearly + 0.08‰ between the suspended particles and the river bedload (average of the Madeira, Solimões, and Beni River).

Statistically significant correlations occur between the Ti and Li isotopic compositions of the river bedload and the suspended river sediments (Fig. 8e). Dellinger et al. (2014) showed that all river bedload sediments had heavier Li isotopic compositions compared to the SPM, which were also finer (smaller size fraction). For nearly all of the samples measured here, the SPM is heavier in Ti isotopic composition compared to the bedload sediments. Lithium isotopes are powerful tracers of silicate weathering, as Li is mobile during water–rock interactions, biologically inert, and its isotopes fractionate during chemical weathering (Lemarchand et al., 2010; Huh et al., 1998). The trend in Li isotopic composition in the Amazon Rivers sediments was interpreted to be due to a mixing of contemporary weathering products mixed with unaltered/pristine bedrock material in the SPM fraction (Dellinger et al., 2014).

Radiogenic strontium (Sr) isotopes are frequently used as tracers of sediment provenance (Grousset and Biscaye, 2005), as variations in geologic history and ages of crustal protoliths impart unique isotopic compositions towards the sediment derived from them. Nearly all of the river suspended sediments from the Amazon River tributaries are relatively close in composition to one another within a given river, and have higher $^{87}Sr/^{86}Sr$ isotopic compositions compared to their river bedload counterparts (Fig. 8f). While Sr isotope data are only available for the Solimões and Madeira Rivers, the Sr and Ti isotopic offset between the river bedload and suspended river sediments is larger for the Madeira. This may be attributed to greater influences of sediment size sorting processes in the Madeira, as it is primarily draining sedimentary rocks compared to arc-derived andesite in the Solimões. Measurable fractionation of radiogenic Sr isotopic compositions of sediments based on size has been observed in other studies focusing on rivers (Goldstein and Jacobsen, 1987), and based on the Ti isotopic fractionation observed with other geochemical proxies (see Fig. 8), it could be the primary cause of the trends observed here.

5.3.2.2. Icelandic river sediments. As described above, a potential source of Ti isotopic fractionation is mineral sorting during fluvial transport, and the ratio of Al_2O_3/TiO_2 should reflect this sorting. Titanium is typically hosted in chemically resistant minerals such as rutile and ilmenite. These Fe,Ti- oxides are isotopically lighter than other minerals, such that the preferential removal of Fe,Ti- oxides due to hydrodynamic sorting can shift the δ^{49}Ti compositions of remaining fine-grained sediments towards heavier Ti isotopic compositions, as proposed by Klaver et al. (2021). The Ti isotopic composition of sediments measured here correlates with the ratio of Al_2O_3/TiO_2 (Fig. 10b), but also correlates well with the Th/Sc ratio, which is a useful tracer for determining precursor compositions of detrital sediments (Fig. 10d). Eastern Mediterranean Sea sediments are defined by different trends compared to the Icelandic sediments, likely due to both Icelandic and Mediterranean sediments having unique endmember compositions. We conclude that sorting is not the primary driver of the δ^{49}Ti isotopic variability observed in the Icelandic sediments, as trends with geochemical

indicators of provenance composition (e.g., Th/Sc) are observed in our samples.

5.4. Influence of mixing in Icelandic sediments

Comparing the Ti isotopic variability of Icelandic volcaniclastic rocks and river sediment with respect to proxies for igneous differentiation and physical size sorting allows us to probe the sensitivity of isotopic composition to crustal composition versus sorting during fluvial transport. The average Ti isotopic composition of Icelandic river sediment is δ^{49}Ti=+0.134 ± 0.06‰, which is lower than modern (<3.5 Ga) shale compositions (δ^{49}Ti = 0.183 ± 0.05‰, Greber at al. 2017a), and higher than average mid-ocean ridge basalt (δ^{49}Ti = 0.002‰, Millet et al., 2016). The δ^{49}Ti and SiO_2 compositions of the Icelandic sediments are shown relative to those of igneous rocks from different geodynamic settings in Fig. 10a.

The behavior of δ^{49}Ti with respect to SiO_2 content in the Icelandic sediments is close to the calc-alkaline trend for igneous rocks (Fig. 10a). Mixing curves calculated between mafic and felsic Icelandic tholeiitic end members replicates the observed compositions of the Icelandic sediments (Fig. 10). Although constraints on the end member compositions are not precise (we use Hekla volcano and Heiðarsporðar ridge compositions), it appears that the effects of grain size (hydrodynamic) sorting, using the proxies of Al_2O_3/TiO_2 and Zr/TiO_2, on the observed Ti isotopic composition are secondary to mixing between mafic and felsic end members (Fig. 10b, c).

The ratio of Al_2O_3/TiO_2 tracks not only fluvial transport (e.g., mineral sorting) processes, but also sediment provenance, as felsic and mafic rocks and calc-alkaline versus tholeiitic igneous suites impart unique Al_2O_3/TiO_2 ratios to sediments derived from them (see Fig. 10b; and Greber et al., 2019). Moreover, the Ti isotopic composition of Icelandic sediments does not correlate with the chemical index of alteration (Fig. S4). Thus, based on the trends observed here and their similarity to mixing trends and isotopic and geochemical compositions of diverse intraplate igneous rocks (Fig. 10b), it is likely that the shifts in Ti isotopic composition result from provenance differences (sediment mixing) rather than chemical weathering.

Additional chemical discriminators can provide insight into whether density sorting of zircon during transport has impacted bulk sediment geochemical composition. Here we have plotted the δ^{49}Ti isotopic compositions with respect to Zr/TiO_2 and Th/Sc (Fig. 10c, d). The correlation between δ^{49}Ti vs. Zr/TiO_2 and Th/Sc indicates that the isotopic trend observed here results from mixing between felsic end members and compositionally diverse mafic end members, therefore the underlying cause of Ti isotopic fractionation observed in the Icelandic sediments is likely mixing of sediments derived from these two sources. Because the Icelandic sediment data follow the magmatic array of Icelandic igneous rocks, this would suggest that either the sediments are sourced from a restricted provenance dominated by one geochemical composition, or reflect mixing of sediment sourced from rocks at various stages of magmatic differentiation. As the samples measured here span a broad geographical portion of Iceland (Fig. 1c), a sediment source of restricted geochemical composition is unlikely. This interpretation should be taken with caution however, as our analysis does not include the composition of suspended river sediment. In the case of river suspended load the hydrodynamic sorting of clay-sized sediments versus coarser sediments may manifest differently, as seen in the Amazon basin sediments. Whether similar processes are at play in Iceland should be the topic of future investigations.

6. Conclusions

To assess how chemical weathering and physical transport processes impact Ti isotope variability in the detrital sediment record, we analyzed Ti isotope ratios in diverse samples representing many different geographic locations and climates within Earth's Critical Zone: loess from around the world; suspended river sediment and bedload from tributaries of the Amazon River; weathering profiles in South Carolina and Oregon, USA; and river sediment and volcaniclastic rocks from Iceland. The Ti isotopic composition of loess is δ^{49}Ti = + 0.132 ± 0.03‰, which is lower than the average composition of modern (<3.5 Ga) shales (δ^{49}Ti ≈ +0.183 ± 0.05‰, Greber et al., 2017). Our loess data show that there are minor trends in δ^{49}Ti with respect to broad geographic locations, which indicates that loess δ^{49}Ti isotopic compositions should be a reasonable proxy for the average upper continental crust composition. The δ^{49}Ti of Amazon River sediments are influenced by physical transport (e.g., hydrodynamic size sorting), with bedload sediment consistently isotopically lighter than suspended sediment, likely due to a higher proportion of denser, Fe,Ti-oxides in the bedload.

Two separate weathering profiles in different climatic regimes and underlying lithology were analyzed to determine the impact of chemical weathering on Ti isotopic fractionation. We found that saprolites developed on a metadiabase dike within a granite quarry in South Carolina had no discernible trends in Ti isotopic composition. By contrast, bauxites developed on Columbia River basalt showed measurable Ti loss and δ^{49}Ti isotopic fractionation, with Ti becoming heavier with more intense weathering. This can be modeled using a Rayleigh distillation approach. One anomalous sample falls off this trend (sample 5/1–14, δ^{49}Ti = -0.136 ‰) which may be due to the presence of anatase or Ti-rich ilmenite. Based on the variety of samples from different climatic regimes measured here, crustal protolith composition and physical sorting during transport appear to have a stronger control on the Ti isotopic composition compared to chemical weathering processes.

When using δ^{49}Ti in detrital sediments for reconstructing the bulk continental crust composition, comparison with trace element data can provide information about whether the samples have been influenced by intense chemical weathering, physical transport processes or mixing of sediments from different rock types. Such processes may fractionate Ti isotopes, leading to a skewed estimate of crust composition.

Declaration of Competing Interest

The authors declare that they have no known competing financial interests or personal relationships that could have appeared to influence the work reported in this paper.

Acknowledgments

This work was supported by the Ford Foundation Fellowship to S.M. A., NASA grants NNX17AE86G, NNX17AE87G, 80NSSC17K0744, 80NSSC20K0821, 80NSSC20K1409, and NSF grant EAR-2001098 to N. D. NDG acknowledges support by the Swiss National Science Foundation (grant 181172). We thank J. Hu, X. Chen, N. Nie for their assistance with mass spectrometry, and discussions with Z. Zhang and A. Johnson were greatly appreciated. We also acknowledge the help of L. Armingeon and T. Pettke for LA-ICP-MS analysis. The manuscript was improved through the constructive comments of the reviewers, associate editor, and executive editor. We also thank the UC Anza Borrego Reserve for facilities during the writing of this manuscript.

Appendix A. Supplementary material

The following are the Supplementary data to this article:

Supplementary Figure S1: Strontium and neodymium isotopic compositions of loess with respect to stable titanium isotope compositions. Supplementary Figure S2: Elemental ratios of Amazon River sediment and bedload relative to the Andes rock average, average upper continental crust, average shales, and individual igneous rocks. Supplemental Figure S3: Elemental spectra from TEM analysis of bauxite samples. Supplemental Figure S4: Chemical index of alteration of Icelandic volcaniclastic rocks and river sediment with respect to titanium isotopic

compositions. Supplemental Figure S5: Chemical index of alteration of saprolite samples with respect to stable titanium isotope compositions. Supplementary table S1: Major and trace element compositions of Icelandic river sediments. Supplementary table S2: Mixing model end-members with geochemical and titanium isotopic compositions of Icelandic rocks. Supplementary table S3: Geochemical compositions of igneous rocks from the Andes. Supplementary table S4: Geochemical compositions of igneous rocks from Iceland.

Supplementary material to this article can be found online at https://doi.org/10.1016/j.gca.2023.05.008.

References

Aarons, S.M., Aciego, S.M., Gleason, J.D., 2013. Variable Hf-Sr-Nd radiogenic isotopic compositions in a Saharan dust storm over the Atlantic: Implications for dust flux to oceans, ice sheets and the terrestrial biosphere. Chem. Geol. 349, 18–26.

Aarons, S.M., Reimink, J.R., Greber, N.D., Heard, A.W., Zhang, Z., Dauphas, N., 2020. Titanium isotopes constrain a magmatic transition at the Hadean-Archean boundary in the Acasta Gneiss Complex. Sci. Adv. 6, eabc9959.

Aarons, S.M., Dauphas, N., Blanchard, M., Zeng, H., Nie, N.X., Johnson, A.C., Greber, N. D., Hopp, T., 2021. Clues from *Ab Initio* Calculations on Titanium Isotopic Fractionation in Tholeiitic and Calc-Alkaline Magma Series. ACS Earth Space Chem. 5, 2466–2480.

Alcott, L.J., Mills, B.J., Bekker, A., Poulton, S.W., 2022. Earth's great oxidation event facilitated by the rise of sedimentary phosphorus recycling. Nat. Geosci. 15, 210–215.

Anand, R.R., Gilkes, R.J., 1984. Weathering of ilmenite in a lateritic pallid zone. Clays. Clay. Miner. 32, 363–374.

Barling, J., 1990. The petrogenesis of the newer lavas of Heard Island, Southern Indian Ocean. Monash University. Ph.D. thesis.

Barling, J., Goldstein, S.L., Nicholls, I.A., 1994. Geochemistry of Heard Island (southern Indian Ocean): characterization of an enriched mantle component and implications for enrichment of the sub-Indian Ocean mantle. J. Petrol. 35, 1017–1053.

Bern, C.R., Chadwick, O.A., Hartshorn, A.S., Khomo, L.M., Chorover, J., 2011. A mass-balance model to separate and quantify colloidal and solute redistributions in soil. Chem. Geol. 282, 113–119.

Berner, E.K., Berner, R.A., 1987. The Global Water Cycle. Prentice-Hall, Upper Saddle River, New Jersey.

Berner, R.A., Lasaga, A.C., Garrels, R.M., 1983. The carbonate-silicate geochemical cycle and its effect on atmospheric carbon dioxide over the past 100 million years. Am. J. Sci. 283, 641–683.

Bindeman, I.N., Gurenko, A.A., Carley, T., Miller, C., Martin, E., Sigmarsson, O., 2012. Silicic magma petrogenesis in Iceland by remelting of hydrothermally altered crust based on oxygen isotope diversity and disequilibria between zircon and magma with implications for MORB. Terra Nova 24, 227–232.

Bouchez, J., Lajeunesse, E., Gaillardet, J., France-Lanord, C., Dutra-Maia, P., Maurice, L., 2010. Turbulent mixing in the Amazon River: The isotopic memory of confluences. Earth Planet. Sci. Lett. 290, 37–43.

Bouchez, J., Lupher, M., Gaillardet, J., France-Lanord, C., Maurice, L., 2011a. How important is it to integrate riverine suspended sediment chemical composition with depth? Clues from Amazon River depth-profiles. Geochim. Cosmochim. Acta 75, 6955–6970.

Bouchez, J., Métivier, F., Lupker, M., Maurice, L., Perez, M., Gaillardet, J., France-Lanord, C., 2011b. Prediction of depth-integrated fluxes of suspended sediment in the Amazon River: particle aggregation as a complicating factor. Hydrol. Process. 25, 778–794.

Bouchez, J., Gaillardet, J., France-Lanord, C., Maurice, L., Dutra-Maia, P., 2011c. Grain size control of river suspended sediment geochemistry: Clues from Amazon River depth profiles. Geochem. Geophys. 12, Q03008.

Bouchez, J., Galy, V., Hilton, R.G., Gaillardet, J., Moreira-Turcq, P., Pérez, M.A., France-Lanord, C., Maurice, L., 2014. Source, transport and fluxes of Amazon River particulate organic carbon: Insights from river sediment depth-profiles. Geochim. Cosmochim. Acta 133, 280–298.

Brewer, R., 1964. Fabric and Mineral Analysis of Soils. John Wiley, New York.

Brimhall, G.H., Dietrich, W.E., 1987. Constitutive mass balance relations between chemical composition, volume, density, and strain in metasomatic hydrothermal systems: results on weathering and pedogenesis. Geochim. Cosmochim. Acta 51, 567–587.

Carley, T.L., Miller, C.F., Wooden, J.L., Padilla, A.J., Schmitt, A.K., Economos, R.C., Bindeman, I.N., Jordan, B.T., 2014. Iceland is not a magmatic analog for the Hadean: Evidence from the zircon record. Earth Planet. Sci. Lett. 405, 85–97.

Carley, T.L., Miller, C.F., Fisher, C.M., Hanchar, J.M., Vervoort, J.D., Schmitt, A.K., Economos, R.C., Jordan, B.T., Padilla, A.J., Banik, T.J., 2020. Petrogenesis of Silicic Magmas in Iceland through Space and Time: The Isotopic Record Preserved in Zircon and Whole Rocks. J. Geol. 128 (1), 1–28.

Carlotto, V., Gil, W., Cárdenas, J., Chávez, R., 1996. Geología de los cuadrángulos de Urubamba y Calca, in: A, S. (Ed.), maps 27-4 y 27-s.

Catt, J.A., 2001. The agricultural importance of loess. Earth. Sci. Rev. 54, 213–229.

Chamberlain, K., Barclay, J., Preece, K., Brown, R., Davidson, J., 2019. Lower Crustal Heterogeneity and Fractional Crystallisation Control Evolution of Small Volume Magma Batches at Ocean Island Volcanoes (Ascension Island, South Atlantic). J. Petrol. 60, 1489–1522.

Chauvel, C., Garçon, M., Bureau, S., Besnault, A., Jahn, B.M., Ding, Z., 2014. Constraints from loess on the Hf-Nd isotopic composition of the upper continental crust. Earth Planet. Sci. Lett. 388, 48–58.

Chen, H., Liu, X.M., Wang, K., 2020. Potassium isotope fractionation during chemical weathering of basalts. Earth Planet. Sci. Lett. 539, 116192.

Condie, K.C., 1993. Chemical composition and evolution of the upper continental crust: contrasting results from surface samples and shales. Chem. Geol. 104, 1–37.

Cornu, S., Lucas, Y., Lebon, E., Ambrosi, J.P., Luizao, F., Rouiller, J., Bonnay, M., Neal, C., 1999. Evidence of titanium mobility in soil profile Manaus, central Amazonia. Geoderma 91, 281–295.

Dauphas, N., Pourmand, A., Teng, F.Z., 2009. Routine isotopic analysis of iron by HR-MC-ICPMS: How precise and how accurate? Chem. Geol. 267, 175–184.

Dellinger, M., Gaillardet, J., Bouchez, J., Calmels, D., Galy, V., Hilton, R.G., Louvat, P., France-Lanord, C., 2014. Lithium isotopes in large rivers reveal the cannibalistic nature of modern continental weathering and erosion. Earth Planet. Sci. Lett. 401, 359–372.

Deng, Z., Moynier, F., Sossi, P. A., Chaussidon, M., 2018. Bridging the depleted MORB mantle and the continental crust using titanium isotopes. Geochem.Perspect. Lett. 9, 11–15.

Deng, Z., Chaussidon, M., Savage, P., Robert, F., Pik, R., Moynier, F., 2019. Titanium isotopes as a tracer for the plume or island arc affinity of felsic rocks. Proc. Natl. Acad. Sci. U. S. A. 116, 1132–1135.

Farges, F., Brown, G.E., 1997. Coordination chemistry of titanium (IV) in silicate glasses and melts: IV. XANES studies of synthetic and natural volcanic glasses and tektites at ambient temperature and pressure. Geochim. Cosmochim. Acta 61, 1863–1870.

Fassio, J.M., 1990. Geochemical evolution of ferruginous bauxite deposits in northwestern Oregon and southwestern Washington. Portland State University. M.S. thesis.

Field, L., Blundy, J., Calvert, A., Yirgu, G., 2013. Magmatic history of Dabbahu, a composite volcano in the Afar Rift. Ethiopia. Geol. Soc. Am. Bull. 125, 128–147.

Firdaus, M.L., Minami, T., Norisuye, K., Sohrin, Y., 2011. Strong elemental fractionation of Zr-Hf and Nb-Ta across the Pacific Ocean. Nat. Geosci. 4, 227–230.

Gaillardet, J., Dupré, B., Allègre, C.J., 1999. Global silicate weathering and CO_2 consumption rates deduced from the chemistry of large rivers. Chem. Geol. 159, 3–30.

Gallet, S., Jahn, B.M., Van Vliet Lanoë, B., Dia, A., Rossello, E., 1998. Loess geochemistry and its implications for particle origin and composition of the upper continental crust. Earth Planet. Sci. Lett. 156, 157–172.

Garcia, D., Fonteilles, M., Moutte, J., 1994. Sedimentary Fractionations between Al, Ti, and Zr and the Genesis of Strongly Peraluminous Granites. J. Geol. 102, 411–422.

Gardner, L.R., Kheoruenromne, I., Chen, H.S., 1978. Isovolumetric geochemical investigation of a buried granite saprolite near Columbia, SC, USA. Geochim. Cosmochim. Acta 42, 417–424.

Gardner, L.R., Kheoruenromne, I., Chen, H.S., 1981. Geochemistry and mineralogy of an unusual diabase saprolite near Columbia. South Carolina. Clays Clay Miner. 29, 184–190.

Gibbs, R.J., 1967. The geochemistry of the Amazon River system: Part I. The factors that control the salinity and the composition and concentration of the suspended solids. Geol. Soc. Am. Bull. 78, 1203–1232.

Goldstein, S.J., Jacobsen, S.B., 1987. The Nd and Sr isotopic systematics of river-water dissolved material: implications for the sources of Nd and Sr in seawater. Chem. Geol. 66, 245–272.

Greaney, A.T., Rudnick, R.L., Romaniello, S.J., Johnson, A.C., Gaschnig, R.M., Anbar, A. D., 2020. Molybdenum isotope fractionation in glacial diamictites tracks the onset of oxidative weathering of the continental crust. Earth Planet. Sci. Lett. 534, 116083.

Greaney, A.T., Rudnick, R.L., Romaniello, S.J., Johnson, A.C., Anbar, A.D., Cummings, M.L., 2021. Assessing molybdenum isotope fractionation during continental weathering as recorded by weathering profiles in saprolites and bauxites. Chem. Geol. 566, 120103.

Greber, N.D., Dauphas, N., 2019. The chemistry of fine-grained terrigenous sediments reveals a chemically evolved Paleoarchean emerged crust. Geochim. Cosmochim. Acta 255, 247–264.

Greber, N.D., Dauphas, N., Bekker, A., Ptáček, M.P., Bindeman, I.N., Hofmann, A., 2017a. Titanium isotopic evidence for felsic crust and plate tectonics 3.5 billion years ago. Science 357, 1271–1274.

Greber, N.D., Dauphas, N., Puchtel, I.S., Hofmann, B.A., Arndt, N.T., 2017b. Titanium stable isotopic variations in chondrites, achondrites and lunar rocks. Geochim. Cosmochim. Acta 213, 534–552.

Greber, N.D., Pettke, T., Vilela, N., Lanari, P., Dauphas, N., 2021. Titanium isotopic compositions of bulk rocks and mineral separates from the Kos magmatic suite: Insights into fractional crystallization and magma mixing processes. Chem. Geol. 578, 120303.

Grey, I.E., Reid, A.F., 1975. The structure of pseudorutile and its role in the natural alteration of ilmenite. Am. Miner. 60, 989–1906.

He, X., Ma, J., Wei, G., Wang, Z., Zhang, L., Zeng, T., Zhang, Z., 2022. Mass-dependent fractionation of titanium stable isotopes during intensive weathering of basalts. Earth Planet. Sci. Lett. 579, 117347.

Hoare, L., Klaver, M., Saji, N.S., Gillies, J., Parkinson, I.J., Lissenberg, C.J., Millet, M.A., 2020. Melt chemistry and redox conditions control titanium isotope fractionation during magmatic differentiation. Geochim. Cosmochim. Acta 282, 38–54.

Hoare, L., Klaver, M., Muir, D.D., Klemme, S., Barling, J., Parkinson, I.J., Lissenberg, C.J., Millet, M.-A., 2022. Empirical and experimental constraints on Fe-Ti oxide-melt titanium isotope fractionation factors. Geochim. Cosmochim. Acta 326, 253–272.

Huang, K.-J., Teng, F.-Z., Elsenouy, A., Li, W.-Y., Bao, Z.-Y., 2013. Magnesium isotopic variations in loess: Origins and implications. Earth Planet. Sci. Lett. 374, 60–70.

Huh, Y., Chan, L.-H., Zhang, L., Edmond, J.M., 1998. Lithium and its isotopes in major world rivers: implications for weathering and the oceanic budget. Geochim. Cosmochim. Acta 62, 2039–2051.
Jahn, B.M., Gallet, S., Han, J., 2001. Geochemistry of the Xining, Xifeng and Jixian sections, Loess Plateau of China: eolian dust provenance and paleosol evolution during the last 140 ka. Chem. Geol. 178, 71–94.
Johnson, A.C., Aarons, S.M., Dauphas, N., Nie, N.X., Zeng, H., Helz, R., Romaniello, S.J., Anbar, A.D., 2019. Titanium Isotopic Fractionation in Kilauea Iki Lava Lake Driven by Oxide Crystallization. Geochim. Cosmochim. Acta 264, 180–190.
Jónasson, K., 1994. Rhyolite volcanism in the Krafla central volcano, north-east Iceland. Bull. Volcanol. 56, 516–528.
Jonasson, K., 2007. Silicic volcanism in Iceland: composition and distribution within the active volcanic zones. J. Geodynam. 43, 101–117.
Kasting, J.F., Catling, D., 2003. Evolution of a habitable planet. Annu. Rev. Astron. Astrophys. 41, 429–463.
Kerr, A.C., Aspden, J.A., Tarney, J., Pilatasig, L.F., 2002. The nature and provenance of accreted oceanic terranes in western Ecuador: Geochemical and tectonic constraints. J. Geol. Soc. 159, 577–594.
Klaver, M., Djuly, T., de Graaf, S., Sakes, A., Wijbrans, J., Davies, G., Vroon, P., 2015. Temporal and spatial variations in provenance of Eastern Mediterranean Sea sediments: Implications for Aegean and Aeolian arc volcanism. Geochim. Cosmochim. Acta 153, 149–168.
Klaver, M., MacLennan, S.A., Ibañez-Mejia, M., Tissot, F.L.H., Vroon, P.Z., Miller, M.A., 2021. Reliability of detrital marine sediments as proxy for continental crust composition: The effects of hydrodynamic sorting on Ti and Zr isotope systematics. Geochim. Cosmochim. Acta 310, 221–239.
Kohn, M.J., Miselis, J.L., Fremd, T.J., 2002. Oxygen isotope evidence for progressive uplift of the Cascade Range. Oregon. Earth Planet. Sci. Lett. 204, 151–165.
Large, R.R., Mukherjee, I., Zhukova, I., Corkrey, R., Stepanov, A., Danyushevsky, L.V., 2018. Role of upper-most crustal composition in the evolution of the Precambrian ocean–atmosphere system. Earth Planet. Sci. Lett. 487, 44–53.
Lee, C.-T.-A., Yeung, L.Y., McKenzie, N.R., Yokoyama, Y., Ozaki, K., Lenardic, A., 2016. Two-step rise of atmospheric oxygen linked to the growth of continents. Nat. Geosci. 9, 417–424.
Lehnert, K., Su, Y., Langmuir, C.H., Sarbas, B., Nohl, U., 2000. A global geochemical database structure for rocks. Geochem. Geophys. Geosyst. 1, 1012.
Lemarchand, E., Chabaux, F., Vigier, N., Millot, R., Pierret, M.-C., 2010. Lithium isotope systematics in a forested granitic catchment (Strengbach, Vosges Mountains, France. Geochim. Cosmochim. Acta 74, 4612–4628.
Li, W.-Y., Teng, F.-Z., Ke, S., Rudnick, R.L., Gao, S., Wu, F.-Y., Chappell, B.W., 2010. Heterogeneous magnesium isotopic composition of the upper continental crust. Geochim. Cosmochim. Acta 74, 6867–6884.
Liu, X.-M., Rudnick, R.L., McDonough, W.F., Cummings, M.L., 2013. Influence of chemical weathering on the compositions of the continental crust: Insights from Li and Nd isotopes in bauxite profiles developed on Columbia River Basalts. Geochim. Cosmochim. Acta 115, 73–91.
Liu, S.A., Teng, F.-Z., Li, S., Wei, G.J., Ma, J.-L., Li, D., 2014a. Copper and iron isotope fractionation during weathering and pedogenesis: insights from saprolite profiles. Geochim. Cosmochim. Acta 146, 59–75.
Liu, X.-M., Teng, F.-Z., Rudnick, R.L., McDonough, W.F., Cummings, M.L., 2014b. Massive magnesium depletion and isotope fractionation in weathered basalts. Geochim. Cosmochim. Acta 135, 336–349.
Mancini, A., Mattsson, H.B., Bachmann, O., 2015. Origin of the compositional diversity in the basalt-to-dacite series erupted along the Heiðarsporður ridge, NE Iceland. J. Volcanol. Geotherm. Res. 301, 116–127.
Mandl, M.B., 2019. Titanium isotope fractionation on the Earth and moon: constraints on magmatic processes and moon formation. ETH Zürich. Ph.D. thesis.
Marsh, B.D., Gunnarsson, B., Congdon, R., Carmody, R., 1991. Hawaiian basalt and Icelandic rhyolite: indicators of differentiation and partial melting. Int. J. Earth Sci. 80, 481–510.
Martin, E., Martin, H., Sigmarsson, O., 2008. Could Iceland be a modern analogue for the Earth's early continental crust? Terra Nova 20, 463–468.
Martin, J.-M., Meybeck, M., 1979. Elemental mass-balance of material carried by major world rivers. Mar. Chem. 7, 173–206.
Millet, M.A., Dauphas, N., 2014. Ultra-precise titanium stable isotope measurements by double-spike high resolution MC-ICP-MS. J. Anal. At. Spectrom. 29, 1444–1458.
Millet, M.A., Dauphas, N., Greber, N.D., Burton, K.W., Dale, C.W., Debret, B., Macpherson, C.G., Nowell, G.M., Williams, H.M., 2016. Titanium stable isotope investigation of magmatic processes on the Earth and Moon. Earth Planet. Sci. Lett. 449, 197–205.
Morgan, W.J., 1971. Convection Plumes in the Lower Mantle. Nature 230, 42–43.
Nesbitt, H.W., 1979. Mobility and fractionation of rare earth elements during weathering of a granodiorite. Nature 279, 206–210.
Orians, K.J., E.A., B., Bruland, K.W., 1990. Dissolved titanium in the open ocean. Nature 348, 322-325.
Ott, E.-J.-E., Kucinski, T.M., Dawson, J.N., Freedman, M.A., 2021. Use of Transmission Electron Microscopy for Analysis of Aerosol Particles and Strategies for Imaging Fragile Particles. Anal. Chem. 93, 11347–11356.
Peters, D., Pettke, T., 2016. Evaluation of Major to Ultra Trace Element Bulk Rock Chemical Analysis of Nanoparticulate Pressed Powder Pellets by LA-ICP-MS. Geostand. Geoanal. Res. 41, 5–28.
Ptáček, M.P., Dauphas, N., Greber, N.D., 2020. Chemical evolution of the continental crust from a data-driven inversion of terrigenous sediment compositions. Earth Planet. Sci. Lett. 539, 116090.
Putzer, H., 1984. The geological evolution of the Amazon Basin and its mineral resources. In: Sioli, H. (Ed.), The Amazon: Limnology and Landscape Ecology of a Mighty Tropical River and its Basin. The Netherlands, Dordrecht, pp. 15–46.
Reidel, S.P., 1983. Stratigraphy and petrogenesis of the Grande Ronde Basalt from the deep canyon country of Washington, Oregon, and Idaho. Geol. Soc. Am. Bull. 94, 519–542.
Reidel, S.P., Tolan, T.L., Hooper, P.R., Beeson, M.H., Fecht, K.R., Bentley, R.D., Anderson, J.L., 1989. The Grande Ronde Basalt, Columbia River Basalt Group; stratigraphic descriptions and correlations in Washington, Oregon, and Idaho. In: Reidel, S.P., Hooper, P.R. (Eds.), Volcanism and tectonism in the Columbia River floodbasalt province. Geological Society of America (GSA), Boulder, CO, United States, pp. 21–53.
Reimink, J.R., Chacko, T., Stern, R.A., Heaman, L.M., 2014. Earth's earliest evolved crust generated in an Iceland-like setting. Nat. Geosci. 7, 529–533.
Rezende, G.L., Martins, C.M., Nogueira, A.C.R., Domingos, F.G., Ribeiro-Filho, N., 2021. Evidence for the Central Atlantic magmatic province (CAMP) in Precambrian and Phanerozoic sedimentary basins of the southern Amazonian Craton. Brazil. J. South Am. Earth Sci. 108, 103216.
Rudnick, R.L., Gao, S., 2003. Composition of the continental crust. Treatise on geochemistry 3, 1–64.
Rudnick, R.L., Tomascak, P.B., Njo, H.B., Gardner, L.R., 2004. Extreme lithium isotopic fractionation during continental weathering revealed in saprolites from South Carolina. Chem. Geol. 212, 45–57.
Rzehak, L.J.A., Kommescher, S., Kurzweil, F., Sprung, P., Leitzke, F.P., Fonseca, R.O.C., 2021. The redox dependence of titanium isotope fractionation in synthetic Ti-rich lunar melts. Contrib. Mineral. Petrol. 176, 19.
Rzehak, L.J.A., Kommescher, S., Hoare, L., Kurzweil, F., Sprung, P., Leitzke, F.P., Fonseca, R.O.C., 2022. Redox-dependent Ti stable isotope fractionation on the Moon: implications for current lunar magma ocean models. Contrib. Mineral. Petrol. 177, 81.
Savage, P.S., Georg, R.B., Williams, H.M., Burton, K.W., Halliday, A.N., 2011. Silicon isotope fractionation during magmatic differentiation. Geochim. Cosmochim. Acta 75, 6124–6139.
Sigmarsson, O., Hémond, C., Condomines, M., Fourcade, S., Oskarsson, N., 1991. Origin of silicic magma in Iceland revealed by Th isotopes. Geology 19, 621–624.
Sigmarsson, O., Steinthórsson, S., 2007. Origin of Icelandic basalts: a review of their petrology and geochemistry. J. Geodynam. 43, 87–100.
Skrabal, S.A., 1995. Distributions of dissolved titanium in Chesapeake Bay and the Amazon River Estuary. Geochim. Cosmochim. Acta 59, 2449–2458.
Smit, M.A., Mezger, K., 2017. Earth's early O_2 cycle suppressed by primitive continents. Nat. Geosci. 10, 788.
Taboada, T., Cortizas, A.M., Garcia, C., Garcia-Rodeja, E., 2006. Particle-size fractionation of titanium and zirconium during weathering and pedogenesis of granitic rocks in NW Spain. Geoderma 131, 218–236.
Tang, M., Chen, K., Rudnick, R.L., 2016. Archean upper crust transition from mafic to felsic marks the onset of plate tectonics. Science 351, 372–375.
Taylor, S.R., McLennan, S.M., 1985. The continental crust: its composition and evolution. Blackwell Scientific, Oxford.
Taylor, S.R., McLennan, S.M., McCulloch, M.T., 1983. Geochemistry of loess, continental crustal composition and crustal model ages. Geochim. Cosmochim. Acta 47, 1897–1905.
Teng, F.-Z., Li, W.-Y., Rudnick, R.L., Gardner, L.R., 2010. Contrasting lithium and magnesium isotope fractionation during continental weathering. Earth Planet. Sci. Lett. 300, 63–71.
Teng, F.-Z., Hu, Y., Ma, J.-L., Wie, G.-J., Rudnick, R.L., 2020. Potassium isotope fractionation during continental weathering and implications for global K isotopes balance. Geochim. Cosmochim. Acta 278, 261–271.
Thompson, A., Chadwick, O.A., Rancourt, D.G., Chorover, J., 2006. Iron-oxide crystallinity increases during soil redox oscillations. Geochim. Cosmochim. Acta 70, 1710–1727.
Thordarson, T., Hoskuldsson, A., 2002. Iceland (Classic Geology in Europe). Dunedin Academic Press, Edinburgh.
Tian, S., Ding, X., Qi, Y., Wu, F., Cai, Y., Gaschnig, R.M., Xiao, Z., Lv, W., Rudnick, R.L., Huang F. 2023. Dominance of felsic continental crust on Earth after 3 billion years ago is recorded by vanadium isotopes. Proc. Natl. Acad. Sci. U.S.A. 120, e2220563120.
Tian, S., Moynier, F., Inglis, E.C., Rudnick, R.L., Huang, F., Chauvel, C., Creech, J.B., Gaschnig, R.M., Wang, Z., Guo, J.-L., 2021. Zirconium isotopic composition of the upper continental crust through time. Earth Planet. Sci. Lett. 572, 117086.
Tolan, T.L., Reidel, S.P., Beeson, M.H., Anderson, J.L., Fecht, K.R., Swanson, D.A., 1989. Revisions to the estimates of the areal extent and volume of the Columbia River Basalt Group. Volcanism and tectonism in the Columbia River flood-basalt province Geol. Soc. Am. Spec. 239, 1–20.
Viers, J., Dupré, B., Gaillardet, J., 2009. Chemical composition of suspended sediments in World Rivers: New insights from a new database. Sci. Total Environ. 407, 853–868.
Wang, W., Huang, S., Huang, F., Zhao, X., Wu, Z., 2020. Equilibrium inter-mineral titanium isotope fractionation: Implication for high-temperature titanium isotope geochemistry. Geochim. Cosmochim. Acta 269, 540–553.
Weibel, R., 2003. Alteration of detrital Fe-Ti oxides in Miocene fluvial deposits, central Jutland, Denmark. Bull. Geol. Soc. Denmark 50, 171–183.
White, A.F., 2003. Natural weathering rates of silicate minerals. In: Drever, J.I. (Ed.), Treatise on Geochemistry. Elsevier-Pergamon, Oxford, pp. 133–168.
Willbold, M., Hegner, E., Stracke, A., Rocholl, A., 2009. Continental geochemical signatures in dacites from Iceland and implications for models of early Archaean crust formation. Earth Planet. Sci. Lett. 279, 44–52.

Wittman, H., von Blanckenburg, F., Maurice, L., Guyot, J.L., Filizola, N., Kubik, P.W., 2011. Sediment production and delivery in the Amazon River basin quantified by in situ-produced cosmogenic nuclides and recent river loads. Geol. Soc. Am. Bull. 123, 934–950.

Zárate, M., Blasi, A., 1993. Late Pleistocene-Holocene eolian deposits of the southern Buenos Aires province, Argentina: a preliminary model. Quat. Int. 17, 15–20.

Zhang, J., Dauphas, N., Davis, A.M., Pourmand, A., 2011. A new method for MC-ICPMS measurement of titanium isotopic composition: Identification of correlated isotope anomalies in meteorites. J. Anal. At. Spectrom. 26, 2197–2205.

Zhao, X., Tang, S., Li, J., Wang, H., Helz, R., Marsh, B., Zhu, X., Zhang, H., 2020. Titanium isotopic fractionation during magmatic differentiation. Contrib. Mineral. Petrol. 175, 67.